Syntheses, Structural Characterizations, and Optical and Electrochemical Properties of Directly Fused Diporphyrins

Akihiko Tsuda, Hiroyuki Furuta, and Atsuhiro Osuka*

Contribution from the Department of Chemistry, Graduate School of Science, Kyoto University, Sakyo-ku, Kyoto 606-8502, Japan

Received April 30, 2001. Revised Manuscript Received August 1, 2001

Abstract: Directly fused diporphyrins display the extensive π conjugation as evinced by highly perturbed electronic absorption spectra as well as lowered and largely split first oxidation potentials. Such diporphyrins prepared include meso-β doubly linked diporphyrins **7**, meso−meso $\beta-\beta$ $\beta-\beta$ triply linked diporphyrins **8**, and meso−meso $\beta-\beta$ doubly linked diporphyrins **9**. Oxidation of 5,15-diaryl-substituted and 5,10,15-triaryl-substituted Ni^{II}−, Cu^{II}−, and Pd^{II}−porphyrins with tris(4-bromophenyl)aminium hexachloroantimonate (BAHA) in $CHCl_3$ afforded **7**, and triply linked Cu^{II}−diporphyrins **8a** and **8g** were respectively prepared by the oxidation of meso−meso singly linked Cu^{II}−diporphyrins **5c** and **5f** with BAHA. Meso−meso $\beta-\beta$ doubly linked Ni^{II}−diporphyrin **9a** was isolated along with triply linked Ni^{II}−diporphyrin **8e** from the similar oxidation of meso−meso singly linked Ni^{II}−diporphyrin **5a**. Doubly linked diporphyrins **7** and **9a** both exhibit significantly perturbed electronic absorption spectra, in which the Soret-like bands are largely split at around 405−418 and 500−616 nm and the Q-bandlike absorption bands are substantially intensified and red-shifted at 748−820 nm, probably as a consequence of symmetry lowering. Triply linked diporphyrins **8** display more strongly perturbed electronic absorption spectra with split Soret-like bands at 408−419 and 567−582 nm and Q-bandlike absorption bands reaching far-infrared region. Structures of three types of fused diporphyrins **7b** and **7c**, **8g** and **8j**, and **9a** have been unambiguously determined by X-ray crystallography to be nearly coplanar. Both the triply linked diporphyrins **8g** and **8j** exhibit very flat structures, whereas the doubly linked diporphyrins **7b** and **7c** exhibit ruffled structures. The doubly linked diporphyrin **9a** shows a helically twisted conformation with larger ruffling toward the opposite directions and has been actually separated into two enantiomers, which display strong Cotton effects in the CD spectra. The first oxidation potentials (E_{OX1}) decrease in the order of **5** > **7** ≥ **9** > **8**, indicating lift-up of HOMO orbital in this order, and split potential differences $\Delta E = E_{OX1} - E_{OX2}$, in turn, increase in the reverse order of **5** < **7**≤ **9** < **8**. The ^{1}H NMR spectra have indicated that the aromatic porphyrin ring current becomes weakened in the order of **5** > **7** > **8**. Collectively, the electronic interactions between the diporphyrins have been concluded to increase in the other of **5** ≪ **7** ≤ **9** < **8**.

Introduction

In recent years, the creation of π-conjugated porphyrin arrays in which the porphyrin π-electronic systems merge to form large supramolecular chromophores has spurred considerable attention because of their remarkable photophysical properties such as high polarizability and high nonlinear optical (NLO) behavior.[1,2] Conjugated porphyrin arrays having a low-energy excited-state extending near-infrared region and thus an extremely low HOMO−LUMO gap are also of current interest for their potential use as a molecular wire.[3] In these studies, one of the central issues is to increase the electronic interaction between the constituent porphyrins and thereby to decrease HOMO−LUMO gap in order to achieve higher electric conductivity. Along this line, a variety of new bridging structures that can enhance the inter-porphyrin conjugation have been intensively exploited.[4−7] A promising and straightforward synthetic strategy is to connect two porphyrins directly with multiple covalent

* Corresponding author. Phone: (+81)75-753-4008. Fax: (+81)75-753-3970. E-mail: osuka@kuchem.kyoto-u.ac.jp.

(1) (a) Chou, J.-H.; Kosal, M. E.; Nalwa, H. S.; Rakow, N. A.; Suslick, K. S. In *The Porphyrin Handbook*; Kadish, K. M., Smith, K. M., Guilard, R., Eds.; Academic Press: Boston, MA, 2000; Vol. 6, p 43. (b) Schwab, P. F. H.; Levin, M. D.; Michl, J. *Chem. Rev.* **1999**, *99*, 1863.

(2) (a) Graça, M.; Vicente, H.; Jaquinod, L.; Smith, K. M. *Chem. Commun.* **1999**, 1771. (b) Anderson, H. L. *Chem. Commun.* **1999**, 2323 and references therein.

(3) (a) Aviram, A.; Ratner, M. A. *Chem. Phys. Lett.* **1974**, *29*, 277. (b) Ward, M. D. *Chem. Ind.* **1996**, 568. (c) Bumm, L. A.; Arnold, J. J.; Cygan, M. T.; Dunbar, T. D.; Burgan, T. P.; Jones, L.; Allara, D. L.; Tour, J. M.; Weiss, P. S. *Science* **1996**, *271*, 1705. (d) Chen, J.; Reed, M. A.; Rawlett, A. M.; Tour, J. M. *Science* **1999**, *286*, 1550. (e) Joachim, C.; Gimzewski, J. K.; Aviram, A. *Nature* **2000**, *408*, 541.

(4) (a) Arnold, D. P.; Johnson, A. W.; Mahendran, M. *J. Chem. Soc., Perkin Trans 1* **1978**, 366. (b) Arnold, D. P.; Heath, G. A. *J. Am. Chem. Soc.* **1993**, *115*, 12197. (c) Arnold, D. P.; Heath, G. A.; James, D. A. *J. Porphyrins Phthalocyanines* **1999**, *3*, 5.

(5) (a) Lin, V. S.-Y.; DiMagno, S. G.; Therien, M. J. *Science* **1994**, *264*, 1105. (b) Lin, V. S.-Y.; Therien, M. J. *Chem. Eur. J.* **1995**, *1*, 645.

(6) (a) Anderson, H. L. *Inorg. Chem.* **1994**, *33*, 972. (b) Taylor, P. N.; Wylie, A. P.; Huuskonen, W. J.; Anderson, H. L. *Angew. Chem., Int. Ed.* **1998**, *37*, 986. (c) Wilson, G. S.; Anderson, H. L. *Chem. Commun.* **1999**, 1539. (c) Blake, I. M.; Rees, L. H.; Claridge, T. D. W.; Anderson, H. L. *Angew. Chem., Int. Ed.* **2000**, *39*, 1818.

(7) (a) Wagner, R. W.; Johnson, T. E.; Lindsey, J. S. *J. Am. Chem. Soc.* **1996**, *118*, 11166. (b) Burrell, A. K.; Officer, D. L. *Synlett* **1998**, 1297. (c) Martin, R. E.; Diederich, F. *Angew. Chem., Int. Ed.* **1999**, *38*, 1350. (d) Higuchi, H.; Shinbo, M.; Usuki, M.; Takeuchi, M.; Hasegawa, Y.; Tani, K.; Ojima, J. *Bull. Chem. Soc. Jpn.* **1999**, *72*, 1887. (e) Jiang, B.; Yang, S,-W.; Barbini, D. C.; Jones, W. E., Jr. *Chem. Commun.* **1998**, 213. (f) Mongin, O.; Papamicael, C.; Hoyler, N.; Gossauer, A. *J. Org. Chem.* **1998**, *63*, 5568. (g) Schultz, D. A.; Gwaltney, K. P.; Lee, H. *J. Org. Chem.* **1998**, *63*, 4034. (h) Kristine, K.; Kajanus, J.; Martensson, J.; Albinsson, B. *J. Phys. Chem. B* **1997**, *103*, 7329. (i) Chen, C.-T.; Yeh, H.-C.; Zhang, X.; Yu, J. *Org. Lett.* **1999**, *1*, 1767.

10.1021/ja0110933 CCC: $20.00 © 2001 American Chemical Society
Published on Web 09/26/2001

bonds in a so-called "fused diporphyrin" manner, which forces a coplanar geometry that should be quite favorable for electronic π conjugation.

There are, however, only a limited number of reports on fused porphyrin arrays so far,[8−12] despite the large number of covalently and noncovalently linked porphyrin arrays made.[1,13,14] In pioneering work, Crossley et al. employed the condensation of a porphyrin-2,3-dione with 1,2,4,5-tetraaminobenzene for the construction of planar fused diporphyrin **1**[8] (Chart 1) and extended their strategy to the synthesis of a tetraporphyrin array with ∼65 Å molecular length.[8c] These arrays are considered to have potential use as a molecular wire by virtue of their rigid shape and conjugated electronic system as evident from their absorption spectra. The promise of this strategy was recommended also from a theoretical point of view.[9] Benzene-bridged fused diporphyrin **2** reported by Kobayashi et al. displayed a red-shifted Q-bandlike absorption at 711 nm, also indicating its conjugated character.[10] Smith et al. devised an efficient synthetic route to directly fused diporphyrin **3** and related longer arrays using a pyrroloporphyrin subunit.[11] They extended this strategy to the synthesis of a two-dimensionally extending cruciform pentaporphyrin array with a long-wavelength absorption band at 774 nm.[11b] The strongly red-shifted absorption bands associated with fused structures suggest the presence of unusually large electronic interaction between the π orbitals on the two macrocycles and further reinforce the potentials of these molecules for optoelectronic applications. Metal coordination was also used to assemble two porphyrins bearing a peripheral enaminoketone function.[12] Diporphyrins thus assembled displayed a decreased optical HOMO−LUMO gap as well as decreased first one-electron oxidation potential.

Recently, we reported that the one-electron oxidation of porphyrins bearing a sterically uncongested meso position such as 5,15-diaryl-substituted and 5,10,15-triaryl-substituted metalloporphyrins constitutes effective synthetic routes to directly

Chart 1. Fused Diporphyrins

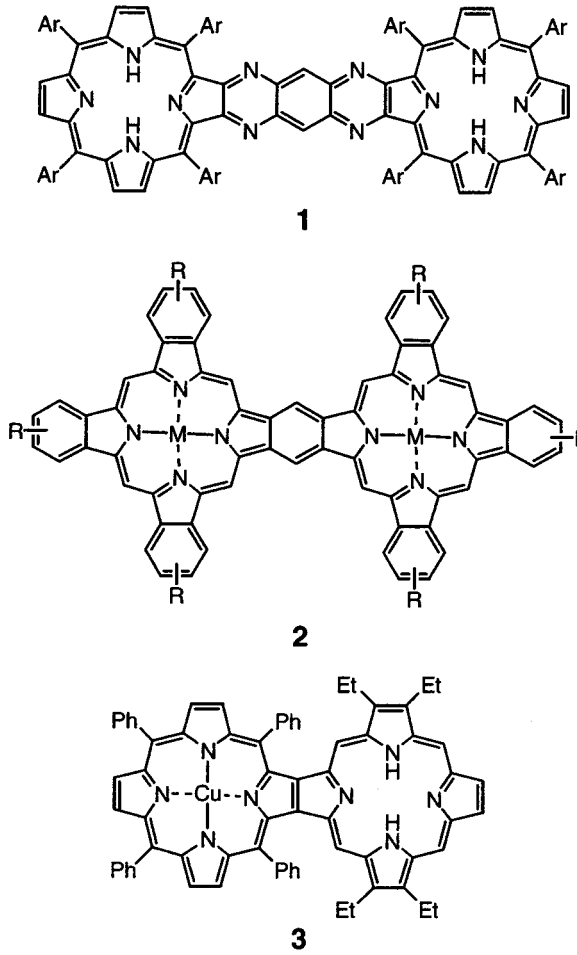

meso−meso and meso-β linked diporphyrins.[15,16] Mg^{II}− and Zn^{II}−porphyrins gave meso−meso linked diporphyrins **5** (Chart 2) by Ag^{I} salt oxidation[15a,b,e,f] or electrochemical oxidation (Scheme 1, path a),[15c] while Cu^{II}−, Ni^{II}−, and Pd^{II}−porphyrins gave meso-β singly linked diporphyrin **6** by electrochemical oxidation (Scheme 1, path b).[17] Both **5** and **6** were expected to take nearly orthogonal conformations, which may explain the relatively weak electronic interaction between the neighboring porphyrin.[17,18] The observed different coupling regioselectivity either giving **5** or **6** may be explained in terms of different HOMO orbital characters. Presumably, Mg^{II}− and

(8) (a) Crossley, M. J.; Burn, P. L. *J. Chem. Soc., Chem. Commun*. **1987**, 39. (b) Crossley, M. J.; Burn, P. L.; Langford, S. J.; Pyke, S. M.; Stark, A. G. *J. Chem. Soc., Chem. Commun.* **1991**, 1567. (c) Crossley, M. J.; Burn, P. L. *J. Chem. Soc., Chem. Commun*. **1991**, 1569. (d) Crossley, M. J.; Govenlock, L. J.; Prasker, J. K. *J. Chem. Soc., Chem. Commun*. **1995**, 2379. (e) Crossley, M. J.; Burn, P. L. Langford, S. J.; Prashar, K. J. *J. Chem. Soc., Chem. Commun*. **1995**, 1921.

(9) Reimers, J. R.; Lü, T. X.; Crossley, M. J.; Hush, N. S. *Chem. Phys. Lett.* **1996**, *256*, 353.

(10) Kobayashi, N.; Numao, M.; Kondo, R.; Nakajima, S.; Osa, T. *Inorg. Chem*. **1991**, *30*, 2241.

(11) (a) Jaquinod, L.; Siri, O.; Khoury, R. G.; Smith, K. M. *Chem. Commun*. **1998**, 1261. (b) Vicente, M. G. H.; Cancilla, M. T.; Lebrilla, C. B.; Smith, K. M. *Chem. Commun*. **1998**, 2355. (c) Paolesse, R.; Jaquinod, L.; Della, S.; Nurco, D. J.; Prodi, L.; Montalti, M.; Natale, C. D.; D'Amico, A.; Carlo, A. D.; Lugli, P.; Smith, K. M. *J. Am. Chem. Soc.* **2000**, *122*, 11295.

(12) Richeter, S.; Jeandon, C.; Ruppert, R.; Callot, H. J. *Chem. Commun*. **2001**, 91.

(13) (a) Maruyama, K.; Osuka, A. *Pure Appl. Chem.* **1990**, *62*, 1511. (b) Wasielewski, M. R. *Chem. Rev.* **1992**, *92*, 435. (c) Kurreck, H.; Huber, M. *Angew. Chem., Int. Ed. Engl.* **1995**, *34*, 849. (d) Wagner, R. W.; Lindsey, J. S. *J. Am. Chem. Soc.* **1994**, *116*, 9759. (e) Collman, J. P.; Anson, F. C.; Barnes, C. E.; Bencosme, S. C.; Geier, T.; Evitt, E. R.; Kreh, R. P.; Meier, K.; Pettman, R. B. *J. Am. Chem. Soc.* **1983**, *105*, 2694. (f) Chang, C. K.; Abdalmuhdi, I. *Angew. Chem., Int. Ed. Engl.* **1984**, *23*, 164. (g) Meier, H.; Kobuke, Y.; Kugimiya, S. *J. Chem. Soc., Chem. Commun.* **1989**, 923. (h) Sessler, J. L.; Hugdall, J.; Martin, M. R. *J. Org. Chem.* **1986**, *51*, 2838. (i) Heiler, D.; McLendon, G.; Rogalskyj, P. *J. Am. Chem. Soc.* **1987**, *109*, 604. (j) Osuka, A.; Maruyama, K. *J. Am. Chem. Soc.* **1988**, *110*, 4454. (k) Brun, A. M.; Harriman, A.; Heitz, V.; Savauge, J. P. *J. Am. Chem. Soc.* **1991**, *113*, 8657. (l) Staab, H. A.; Carell, T. *Angew. Chem., Int. Ed. Engl.* **1994**, *33*, 1466. (m) Segawa, H.; Kunimoto, K.; Susumu, K.; Taniguchi, M.; Shimidzu, T. *J. Am. Chem. Soc.* **1994**, *116*, 11193. (n) Dubowchik, G. M.; Hamilton, A. D. *J. Chem. Soc., Chem. Commun.* **1987**, 293. (o) Mak, C. C.; Bampos, N.; Sanders, J. K. M. *Angew. Chem., Int. Ed. Engl.* **1998**, *37*, 3020. (p) Sugiura, K.; Tanaka, H.; Matsumoto, T.; Kawai, T.; Sakata, Y. *Chem. Lett.* **1999**, 1193.

(14) (a) Imamura, T.; Fukushima, K. *Coord. Chem. Rev.* **2000**, *198*, 133. (b) Wojaczynski, J.; Latos-Grazynski, L. *Coord. Chem. Rev.* **2000**, *204*, 113. (c) Drain, C. M.; Lehn, J.-M. *J. Chem. Soc., Chem. Commun*. **1994**, 2313. (d) Stang, P. J.; Fan, J. Olenyuk, B. *J. Chem. Soc., Chem. Commun*. **1997**, 1453. (e) Kariya, N.; Imamura, T.; Sasaki, Y. *Inorg. Chem.* **1997**, *36*, 833.

(15) (a) Osuka, A.; Shimidzu, H. *Angew. Chem., Int. Ed. Engl.* **1997**, *36*, 135. (b) Yoshida, N.; Shimidzu, H.; Osuka, A. *Chem. Lett.* **1998**, 55. (c) Ogawa, T.; Nishimoto, Y.; Yoshida, N.; Ono, N.; Osuka, A. *Chem. Commun*. **1998**, 337. (d) Yoshida, N.; Aratani, N.; Osuka, A. *Chem. Commun*. **2000**, 197. (e) Aratani, N.; Osuka, A.; Kim, Y. H.; Jeong, D. H.; Kim, D. *Angew. Chem., Int. Ed.* **2000**, *39*, 1458. (f) Yoshida, N.; Osuka, A. *Org. Lett.* **2000**, *2*, 2963.

(16) The syntheses of meso−meso linked diporphyrins were also reported by other groups: (a) Susumu, K.; Shimidzu, T.; Tanaka, K.; Segawa, H. *Tetrahedron Lett*. **1996**, *37*, 8399. (b) Khoury, R. G.; Jaquinod, L.; Smith, K. M. *Chem. Commun.* **1997**, 1057. (c) Wojaczynski, J.; Latos-Grazynski, L.; Chmielewski, P. J.; Calcar, P. V.; Balch, A. L. *Inorg. Chem.* **1999**, *38*, 3040. (d) Senge, M. O.; Feng, X. *Tetrahedron Lett*. **1999**, *40*, 4165. (e) Shi, X.; Liebeskind, L. S. *J. Org. Chem*. **2000**, *65*, 1665. (f) Clausen, C.; Gryko, D. T.; Yasseri, A. A.; Diers, J. R.; Bocian, D. F.; Kuhr, W. G.; Lindsey, J. S. *J. Org. Chem.* **2000**, *65*, 7371.

(17) Ogawa, T.; Nishimoto, Y.; Yoshida, N.; Ono, N.; Osuka, A. *Angew. Chem., Int. Ed.* **1999**, *38*, 176.

Chart 2. Porphyrins Studied in This Paper (Ar = 3,5-Di-*tert*-butylphenyl, Ph = Phenyl)

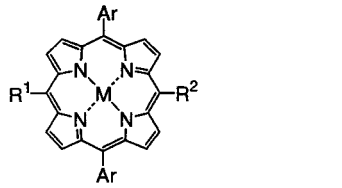

4a ; M=Ni $R^1=R^2=H$
4b ; M=Ni $R^1=H$, $R^2=Ar$
4c ; M=Ni $R^1=Cl$ or Br, $R^2=Ar$
4d ; M=Ni $R^1=H$, $R^2=Cl$
4e ; M=Cu $R^1=H$, $R^2=Ar$
4f ; M=Cu $R^1=Cl$, $R^2=Ar$
4g ; M=Pd $R^1=H$, $R^2=Ar$
4h ; M=Pd $R^1=Br$, $R^2=Ar$
4i ; M=H_2 $R^1=H$, $R^2=Ar$
4j ; M=H_2 $R^1=R^2=Ar$
4k ; M=Zn $R^1=H$, $R^2=Ar$
4l ; M=Zn $R^1=R^2=Ar$

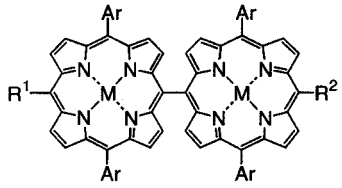

5a ; M=Ni $R^1=R^2=Ar$
5b ; M=Ni $R^1=R^2=Cl$
5c ; M=Cu $R^1=R^2=Ar$
5d ; M=Pd $R^1=H$, $R^2=Br$
5e ; M=Pd $R^1=R^2=Br$
5f ; M=Cu $R^1=R^2=Ph$
5g ; M=H_2 $R^1=R^2=Ar$
5h ; M=Zn $R^1=R^2=Ar$
5i ; M=Pd $R^1=R^2=Ar$

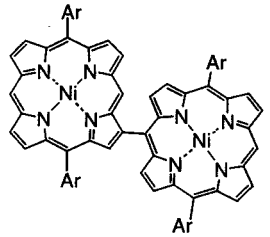

6

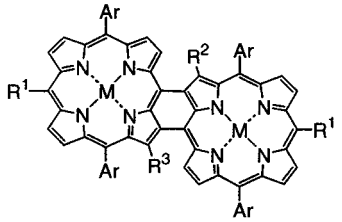

7a ; M=Ni $R^1=Cl$, $R^2=R^3=H$
7b ; M=Ni $R^1=Ar$, $R^2=R^3=H$
7c ; M=Cu $R^1=Ar$, $R^2=R^3=H$
7d ; M=Pd $R^1=Ar$, $R^2=R^3=H$
7e ; M=Pd $R^1=Ar$, $R^2=Cl$, $R^3=H$
7f ; M=Pd $R^1=Ar$, $R^2=R^3=Cl$
7g ; M=H_2 $R^1=Ar$, $R^2=R^3=H$
7h ; M=Zn $R^1=Ar$, $R^2=R^3=H$

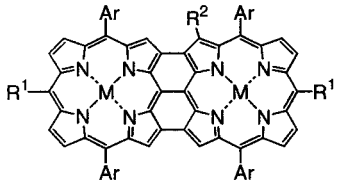

8a ; M=Cu $R^1=Ar$, $R^2=H$
8b ; M=Cu $R^1=Ar$, $R^2=Cl$
8c ; M=H_2 $R^1=Ar$, $R^2=H$
8d ; M=Zn $R^1=Ar$, $R^2=H$
8e ; M=Ni $R^1=Ar$, $R^2=H$
8f ; M=Pd $R^1=Ar$, $R^2=H$
8g ; M=Cu $R^1=Ph$, $R^2=H$
8h ; M=Cu $R^1=Ph$, $R^2=Cl$
8i ; M=H_2 $R^1=Ph$, $R^2=H$
8j ; M=Zn $R^1=Ph$, $R^2=H$
8k ; M=H_2 $R^1=Ar$, $R^2=Cl$
8l ; M=Ni $R^1=Ar$, $R^2=Cl$

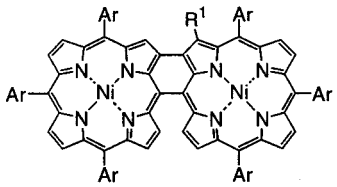

9a ; $R^1=H$
9b ; $R^1=Cl$

Zn^{II}−porphyrins favor A_{2u} HOMO in which there is large electron density at the meso carbon, whereas Cu^{II}−, Ni^{II}−, and Pd^{II}−porphyrins favor A_{1u} HOMO, which has nodal planes through the meso positions and has significant electron density at the β position (Figure 1).[19]

As an extension of these works, we have found novel effective synthetic routes to fused porphyrins through the oxidation of certain metalloporphyins with tris(4-bromophenyl)aminium hexachloroantimonate (BAHA).[20] The oxidation of Cu^{II}−, Ni^{II}−, and Pd^{II}−porphyrins gave rise to formation of meso-β doubly linked diporphyrins **7** (Scheme 1, paths b and c),[20a,21] and the oxidation of meso−meso linked Cu^{II}−diporphyrins **5** gave meso−meso $\beta-\beta$ $\beta-\beta$ triply linked diporphyrins **8**,[20b] probably through meso−meso $\beta-\beta$ doubly linked diporphyrin **9** (Scheme 1, paths d and e). Here we report the syntheses of these three fused diporphyrins, **7**, **8**, and **9**, whose structures have been all characterized by the X-ray crystallography. Their optical and electrochemical properties are also reported with a particular concern about large electronic coupling between diporphyrins.

Results

Meso-β Doubly Linked Diporphyrins 7. BAHA is one of one-electron oxidizing reagents frequently used to generate a

(18) (a) Cho, H. S.; Song, N. W.; Kim, Y. H.; Jeoung, S. C.; Hahn, S.; Kim, d.; Yoshida, N.; Osuka, A. *J. Phys. Chem. A* **2000**, *104*, 3287. (b) Kim, Y. H.; Jeong, D. H.; Kim, D.; Jeoung, S. C.; Cho, H. S.; Kim, S. K.; Aratani, N.; Osuka, A. *J. Am. Chem. Soc.* **2001**, *123*, 76.

(19) Gouterman, M. In *The Porphyrins*; Dolphin, D., Ed.; Academic Press: New York, 1978; Vol. 3, p 1.

(20) (a) Tsuda, A.; Nakano, A.; Furuta, H.; Yamochi, H.; Osuka, A. *Angew. Chem., Int. Ed.* **2000**, *39*, 558. (b) Tsuda, A.; Furuta, H.; Osuka, A. *Angew. Chem., Int. Ed.* **2000**, *39*, 2549.

(21) Analogous meso-β doubly linked diporphyrin was reported to be also formed in the reaction of 5,15-diaryl Ni^{II}−porphyrin with $TeCl_4$: Sugiura, K.; Matsumoto, T.; Ohkouchi, S.; Naitoh, Y.; Kawai, T.; Takai, Y.; Ushiroda, K.; Sakata, Y. *Chem. Commun.* **1999**, 1957.

Scheme 1. Oxidative Transformations of 5,10,15-Triaryl-Substituted Metalloporphyrins (Ar = 3,5-di-*tert*-butylphenyl)

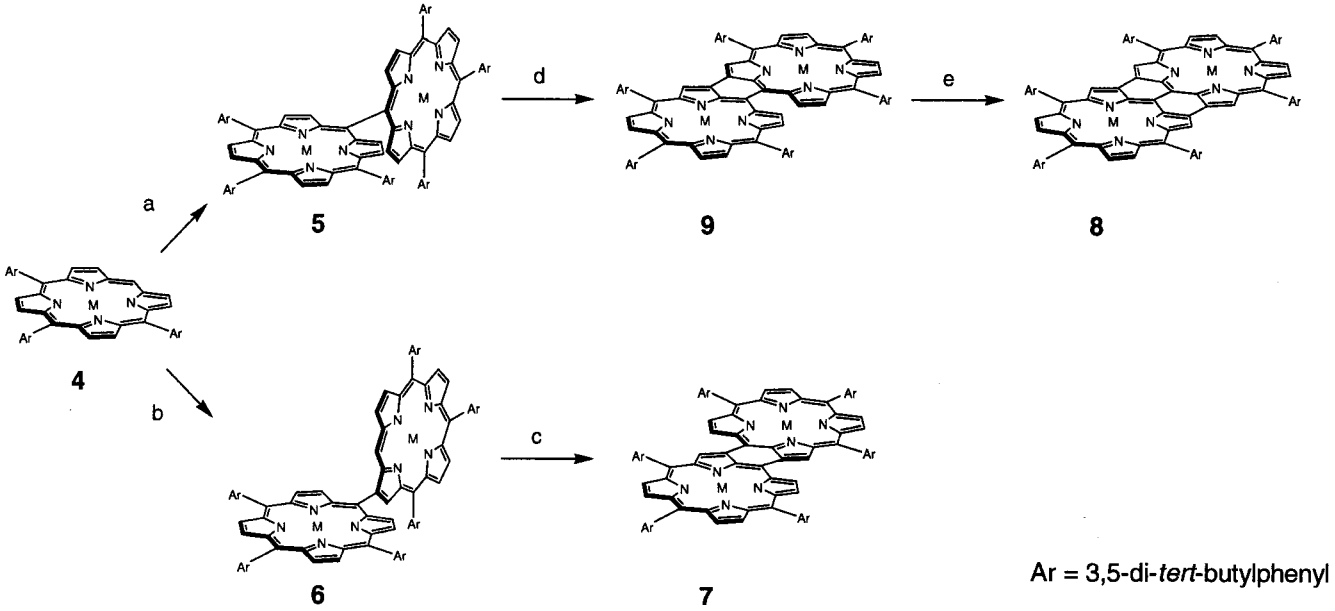

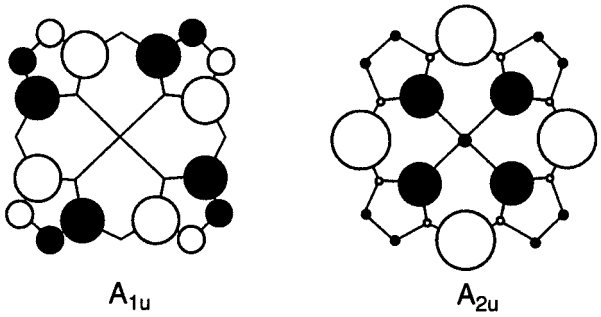

Figure 1. Schematic representation of the two HOMO orbitals of the D_{4h} porphyrin ring.

metalloporphyrin cation radical.[22] We found, however, that one-electron oxidation of 5,15-diaryl-substituted and 5,10,15-triaryl-substituted Ni^{II}−, Cu^{II}−, and Pd^{II}−porphyrins bearing a sterically uncongested meso position with BAHA led to formation of meso-β doubly linked diporphyrins **7**. Initially, 5,15-diaryl-substituted Ni^{II}−porphyrin **4a** was oxidized with an equivalent amount of BAHA in $CHCl_3$ for 12 h. Separation by preparative size exclusion chromatography (SEC) and the analysis by MALDI-TOF mass spectroscopy revealed formation of dimeric, trimeric, tetrameric, and pentameric porphyrins. Subsequent flash chromatography over a silica gel column provided diporphyrin **7a** (11%), which exhibited a parent molecular ion peak at $m/z = 1550$ (calcd for $C_{96}H_{98}N_8Cl_2Ni_2$, 1549) by FAB mass spectrometry and a broad absorption spectrum (λ_{max}-($CHCl_3$) 418, 534, and 756 nm). The 500-MHz ^{1}H NMR spectrum provided three sets of mutually coupled doublets for the peripheral β-protons at 9.42 and 9.11, 9.08 and 8.74, and 8.46 and 8.41 ppm, and a singlet for the β-proton (R^2 and R^3) at 8.98 ppm. A separate BAHA oxidation of meso-β singly linked diporphyrin **6**, which was obtained by the electrochemical oxidation of **4a**,[17] provided **7a** quantitatively, suggesting **6** to be a precursor of **7a**. The obtained higher oligomeric porphyrin arrays formed in the reaction of **4a** with BAHA have been not fully characterized mostly due to their extremely poor solubilities and possible existence of inseparable syn−anti isomers.

(22) (a) Bell, F. A.; Ledwith, A.; Sherrington, D. C. *J. Chem. Soc. C* **1969**, 2719. (b) Smith, K. M.; Barnett, G. H.; Evans, B.; Martynenko, Z. *J. Am. Chem. Soc.* **1979**, *101*, 5939.

To suppress a further coupling reaction, we next examined the oxidation reaction of 5,10,15-trisubstituted porphyrins with a single free meso position. Actually, the oxidation of 5,10,-15-triaryl Ni^{II}−porphyrin **4b** with BAHA afforded **7b** (53%) along with meso-halogenated monomers **4c** (29%) and meso−meso linked diporphyrin **5a** (10%). Similarly, the reaction of **4d** gave **7a** (70%) as a major product together with **5b** (10%).

The oxidation of Cu^{II} complex **4e** with BAHA provided meso-β doubly linked diporphyrin **7c** (25%), meso−meso linked diporphyrin **5c** (33%), and meso-chlorinated monomer **4f** (24%). This result implied that the initial coupling regioselectivity (meso−meso versus meso-β) of Cu^{II}−porphyrin was lower in comparison to that of Ni^{II}−porphyrin. In contrast, the coupling regioselectivity was shown to be quite high for Pd^{II}−porphyrin, in that the oxidation of **4g** gave only meso-β doubly linked diporphyrins **7d** (chlorine free, 20%), **7e** (monochlorinated, 20%), and **7f** (dichlorinated, 19%). The product distribution of **7d**, **7e**, and **7f** was found to depend on the reaction time and the amounts of BAHA used. Thus, the use of 3 equiv of BAHA for 48 h led to the formation of **7f** (49%) as a sole diporphyrin product along with meso-brominated monomer **4h**.[23] Interestingly, the chlorination regioselectivity that was manifest on the basis of the ^{1}H NMR data and the preliminary X-ray analysis (Supporting Information 1) was quite high, only occurring at

(23) In the reaction of Pd^{II}−porphyrin, meso-chlorinated product was not obtained. A possible mechanism for the meso bromination may be bromine atom abstraction by a metalloporphyrin meso radical, since the only available bromine source is BAHA. As described in the text, the oxidation of Ni^{II}−porphyrin **4b** with BAHA gave a .∼1:1 mixture of meso-chlorinated and -brominated monoporphyrins **4c** as side products. Since meso-brominated Ni^{II}−porphyrin was found to undergo a halogen exchange reaction to give meso-chlorinated products under the reaction conditions, it is likely that meso-brominated monoporphyrin was initially formed and was converted to meso-chlorinated porphyrin. In contrast, such a halogen exchange reaction was not observed for Pd^{II}−porphyrins as seen for the reactions of **4g** and **5d**. The observed β chlorination for meso-β doubly linked diporphyrin might be ascribed to steric hindrance of the chlorinated β position or different halogenation mechanism. As suggested by one of the reviewers, we have examined the reaction of **4g** with tris(4-bromophenyl)aminium perchlorate (Bell, F. A.; Ledwith, A.; Sherrington, D. C. *J. Chem. Soc. C* **1969**, 2729) with the aim of suppressing the peripheral β chlorination. But **4g** was recovered after the reaction with tris(4-bromophenyl)aminium perchlorate for 2 days. We have also examined the reaction of **5c** with the percholorate salt, which resulted in the formation of **8g** in a trace amount with the recovery of **5c** (56%) and some insoluble products.

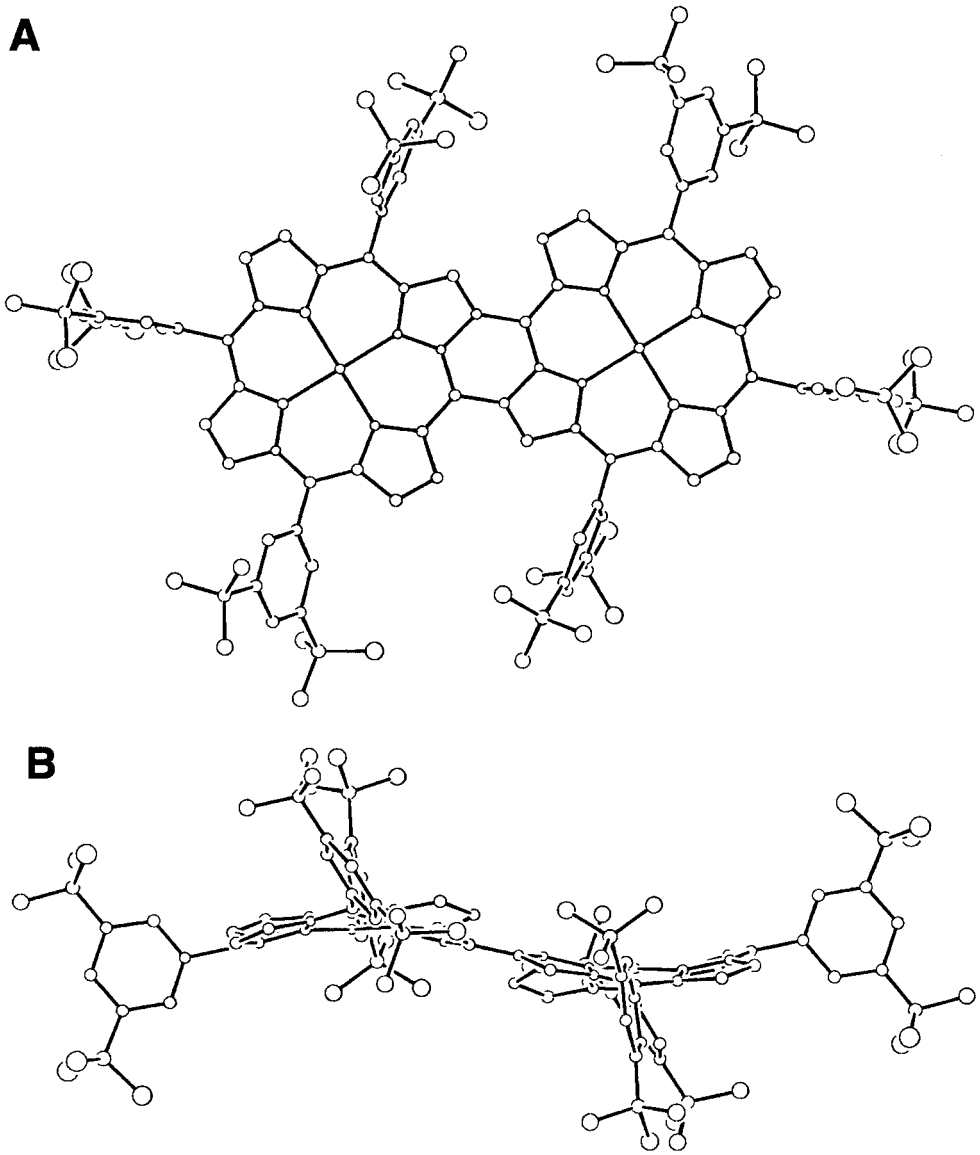

Figure 2. Molecular structures of **7b**. (A) Top view. (B) Side view. Hydrogen atoms have been omitted for clarity.

the β position adjacent to the fused ring. Here it is noteworthy that the fused Cu^{II}−diporphyrin **7c** is a useful precursor for other metalated meso-β doubly linked diporphyrins by virtue of its easy and quantitative transformation into the corresponding free-base diporphyrin **7g**, from which Zn^{II}−diporphyrin **7h** was indeed prepared.

The molecular structures of **7b** and **7c** have been confirmed by X-ray crystallography. In **7b**, the two porphyrin rings are forced to take a nearly coplanar conformation with large ruffling and mean plane deviations of the 25 core atoms of 0.30 Å (Figure 2). The mean Ni−N distance is 1.92 Å, similar to the reported 1.929 Å for Ni^{II}−TPP;[24] the two newly formed meso-β bonds are l.45 Å long, similar to the C_2-C_3 bond length (1.48 Å) of 1,3-butadiene; the Ni−Ni distance is 8.61 Å. The X-ray crystal structure of **7c** also shows almost planar but slightly ruffled conformation with mean plane deviations of 0.26 Å (Figure 3). The meso-β C−C bonds are 1.46 Å long, the Cu−Cu distance is 8.66 Å, and the mean Cu−N distance is 1.98 Å, again similar to the reported Cu−N distance for Cu^{II}−TPP.[24a,25]

The electronic absorption spectra of the meso-β doubly linked diporphyrins **7b**, **7c**, **7d**, **7g**, and **7h** are shown in Figure 4. The absorption spectra display a similar pattern among the series, showing broad and red-shifted three major bands (bands I, II, and III), probably as a reflection of extensive conjugation over the diporphyrin π-electronic system. The positions of bands I (420−430 nm) are quite similar to those of the Soret bands of porphyrin monomers, but the intensities are attenuated compared with those of the porphyrin monomers. Bands II are red-shifted (500−600 nm) relative to bands I and are more broad and complicated, exhibiting several components. Bands III are more red-shifted (750−830 nm) and significantly intensified in comparison to the Q-bands of the porphyrin monomers. The central metals in the porphyrin core have influence on the absorption spectra, particularly on the position of bands III. Those of Ni^{II}− and Pd^{II}−diporphyrins **7b** and **7d** are observed at high-energy positions (756 and 748 nm) and those of Zn^{II}− and free-base diporphyrins **7h** and **7g** are observed at low-energy positions (798 and 820 nm).

(24) (a) Scheidt, W. R. In *The Porphyrin Handbook*; Kadish, K. M., Smith, K. M., Guilard, R., Eds.; Academic Press: Boston, MA, 2000; Vol. 3, p 49. (b) Maclean, A. L.; Foran, G. J.; Kennedy, B. J.; Turner, P.; Hambley, T. W. *Aust. J. Chem.* **1996**, *49*, 1273. (c) Jentzen, W.; Unger, E.; Song, X.-Z.; Jia, S.-L.; Turowska-Tyrk, I.; Schweitzer-Stenner, R.; Dreybrodt, W.; Scheidt, W. R.; Shelnutt, J. A. *J. Phys. Chem. A* **1997**, *101*, 5789.

(25) Fleischer, E. B.; Miller, C. K.; Webb, L. E. *J. Am. Chem. Soc.* **1964**, *86*, 2342.

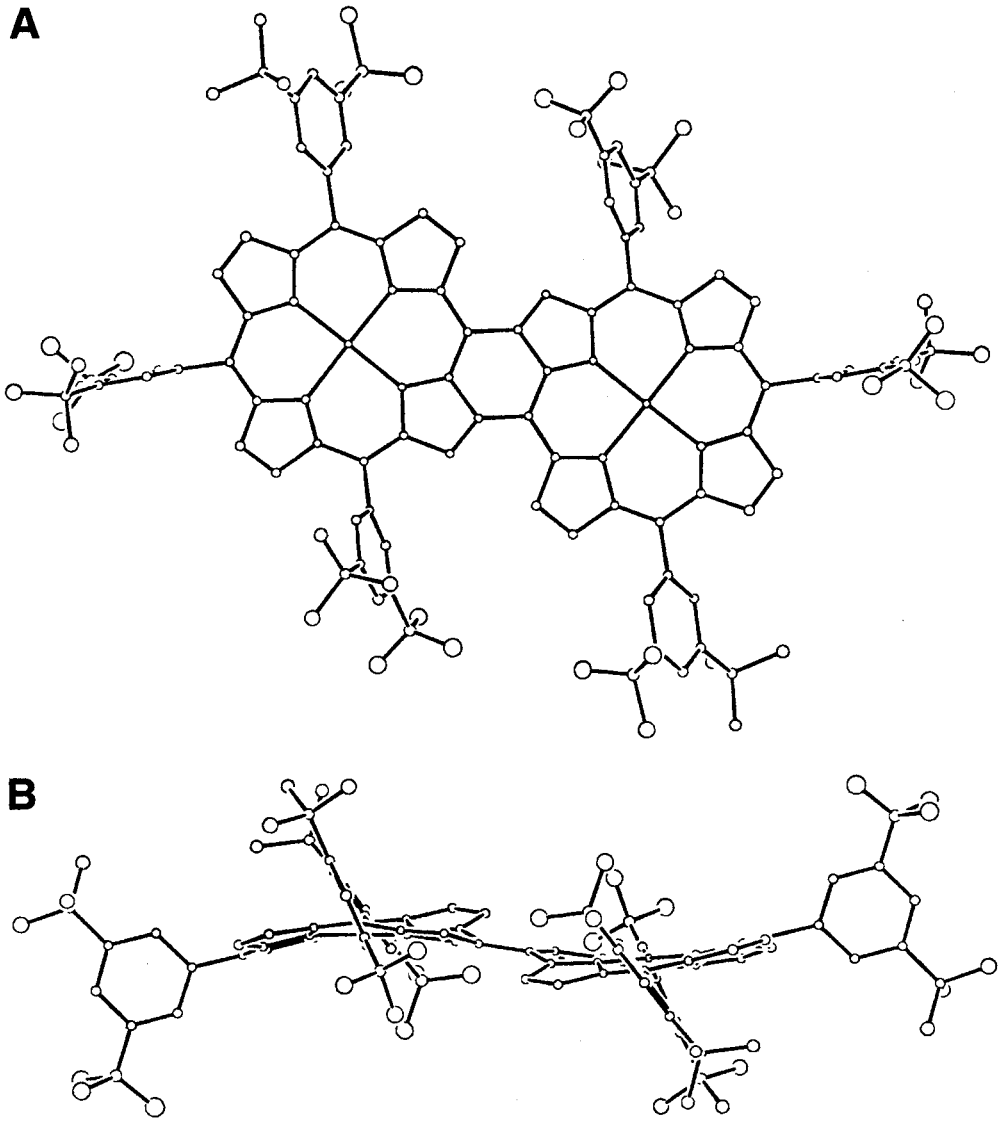

Figure 3. Molecular structures of **7c**. (A) Top view. (B) Side view. Hydrogen atoms have been omitted for clarity.

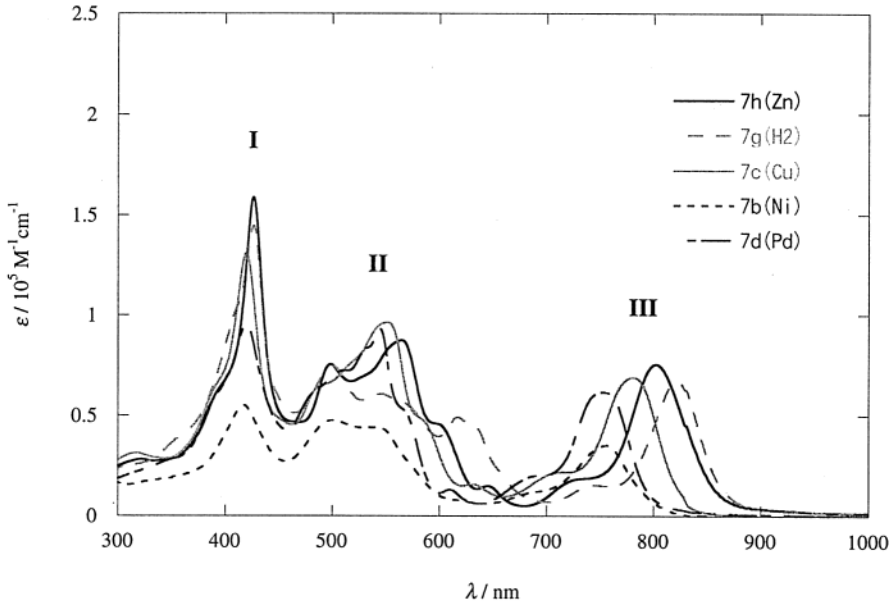

Figure 4. Absorption spectra of meso-β doubly linked diporphyrins in $CHCl_3$.

As an application, meso−meso linked Pd^{II}−diporphyrin **5d** was reacted with BAHA under similar conditions to give tetraporphyrin **7i** (29%) along with meso-brominated porphyrin **5e** (60%) and recovery of **5d** (20%) (Scheme 2). Tetraporphyrin

Scheme 2. Synthesis of Tetraporphyrin **7i** from **5d**

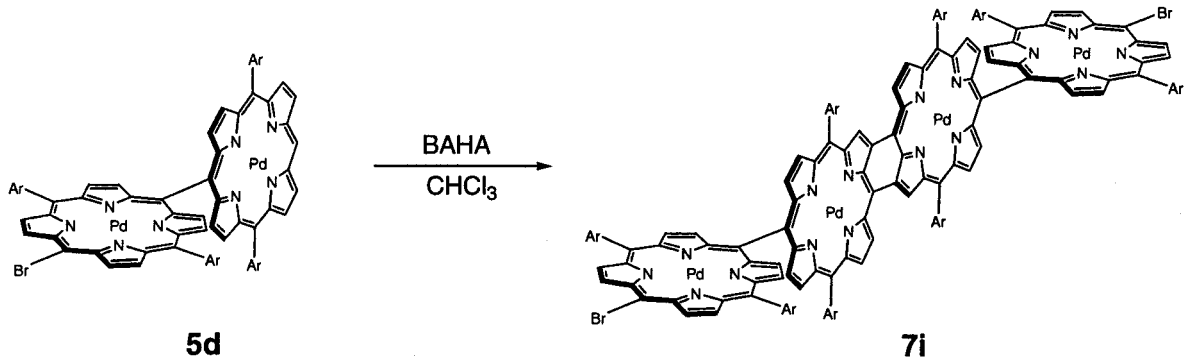

Table 1. Synthesis of **8a** from the Oxidation of **5c** with BAHA.

					yields (%)[a]			
entry	solvent	temp (°C)	time (h)	BAHA (equiv)	**8a**	**8b**	dichlorinated product[b]	**5c**[c]
1	$CHCl_3$	20	12	2	8	29	34	10
2	$CHCl_3$	61	10	2	0	0	58	40
3	$CHCl_3$	0	30	2	5	15	19	60
4	CH_2Cl_2	20	5	2	0	0	0	98
5	THF	20	5	2	0	0	0	96
6	C_6H_6	20	12	2	10	20	14	45
7	$CF_3C_6H_5$	20	30	2	36	34	0	16
8	C_6F_6	20	30	2	55	5	trace	30
9	C_6F_6	20	48	2	62	6	trace	21
10	C_6F_6	20	48	3	74	16	trace	10

[a] Isolated yields. [b] The secondary chlorination site has not been determined. [c] Recovered.

7i exhibits a parent molecular ion peak at $m/z = 3319$ (calcd for $C_{192}H_{198}Br_2N_{16}Pd_4$, 3315) in its MALDI-TOF mass spectrum and absorption spectrum with bands at 419, 554, 752, and 1036 nm (Supporting Information 2). The tetraporphyrin **7i** has an interesting structure possessing both meso−meso single linkage and meso-β fused linkage.

Meso−Meso $\beta-\beta$ $\beta-\beta$ Triply Linked Diporphyrins 8. In the course of these studies, it occurred to us that the oxidation of meso−meso linked metalloporphyrins might lead to formation of meso−meso β-β β-β triply linked diporphyrins. This is more likely for the diporphyrins with an A_{1u} HOMO orbital, since they have a large spin density at the β positions in the cation radical part. In the first attempt, meso−meso singly linked Cu^{II}−diporphyrin **5c** was oxidized with 2 equiv of BAHA in $CHCl_3$ at room temperature for 12 h. Repeated separations over silica gel column chromatography provided triply linked diporphyrins **8a** (chlorine free, 8%) and **8b** (monochlorinated, 29%), together with dichlorinated triply linked diporphyrins (34%) (Table 1, entry 1). The structures of **8a** and **8b** have been suggested by their absorption spectra (**8a**, $\lambda_{max} = 411$, 576, and 996 nm (Figure 7); **8b**, $\lambda_{max} = 409$, 573, and 990 nm) and the parent molecular ion peaks detected by FAB-MS (or MALDI-TOF) (**8a**, $m/z = 1866$, calcd for $C_{124}H_{138}N_8Cu_2$,1865) and (**8b**, $m/z = 1900$, calcd for $C_{124}H_{137}N_8ClCu_2$, 1899). Analogously, the structure of the dichlorinated triply linked diporphyrins has been suggested on the grounds of the molecular weight ($m/z = 1936$, calcd for $C_{124}H_{136}N_8Cl_2Cu_2$, 1933) and the absorption spectrum ($\lambda_{max} = 408$, 571, and 987 nm) that were nearly the same as those of **8a** and **8b**, but its secondary chlorination site has not been determined. In the next step, we attempted to suppress the concurrent peripheral chlorination (Table 1). The chlorination was not suppressed in $CHCl_3$ by temperature variation (entries 1−3), and the ring closure was not effected in CH_2Cl_2 and THF (entries 4 and 5). In C_6H_6 and $CF_3C_6H_5$, we noted some suppression of the peripheral chlorination and slight improvement in the yield of **8a** (entries 6 and 7). These results indicated that the chlorine was coming not only from the solvents but also from the oxidizing reagent, BAHA itself. Meanwhile, we found that the peripheral chlorination was fairly suppressed in C_6F_6, allowing the formation of **8a** in 55% yield (entry 8). Longer reaction time and use of 2−3 equiv of BAHA resulted in the formation of **8a** in 62−74% yield (entries 9 and 10). Cu^{II}−diporphyrin **8a** was synthetically useful, as it was quantitatively demetalated with concentrated H_2SO_4 to give free-base form **8c** from which Zn^{II}−diporphyrin **8d**, Ni^{II}−diporphyrin **8e**, and Pd^{II}−diporphyrin **8f** were prepared.

To confirm the X-ray structure of a parent triply linked fused diporphyrin, we converted meso−meso Cu^{II}−diporphyrin **5f** to triply linked diporphyrins **8g** (chlorine free, 76%; $m/z = 1645$, calcd for $C_{108}H_{106}N_8Cu_2$, 1641) and **8h** (monochlorinated, 6%; $m/z = 1677$, calcd for $C_{108}H_{105}N_8Cu_2Cl$, 1675). The X-ray structure of **8g** is shown in Figure 5. The two porphyrin rings are fused to form a nearly complete coplanar conformation with a very small mean plane deviation (0.03 Å). The C(β)−C(β) bonds are 1.41 Å long and the C(meso)−C(meso) bond is 1.44 Å long; the Cu−Cu distance is 8.38 Å; the mean Cu−N distance is 1.99 Å. It is interesting to note that fused diporphyrin units show nearly orthogonal crystal packing in the solid state with the 3,5-di-*tert*-butylphenyl groups pointing to the Cu^{II}−diporphyrin plane. The Cu^{II}−diporphyrin **8g** was demetalated to free-base diporphyrin **8i**, from which Zn^{II}−diporphyrin **8j** was prepared. The monochlorinated triply linked diporphyrin **8b** was similarly demetalated to **8k.** The orthogonal crystal packing was also observed for the free-base diporphyrin **8k** (Supporting Information 3), whereas Zn^{II}−diporphyrin **8j** displayed a flat structure with a mean plane deviation of 0.23 Å, a Zn−Zn distance of 8.50 Å, a mean Zn−N distance of 2.07 Å, two C(β)−C(β) bonds of 1.44 Å, and the C(meso)−C(meso) bond of 1.51 Å, packed in a parallel manner with the interporphyrin separation of ~5.44 Å (Figure 6). In **8j**, the central Zn^{II} ion has been revealed to coordinate with ethanol (not shown for clarity). The average Zn−N distance observed is slightly longer than the reported 2.037 Å distance of Zn^{II}−TPP.[26]

The electronic absorption spectra of the triply linked diporphyrins are shown in Figure 7. As in the case of the meso-β doubly linked diporphyrins, all the spectra feature three major bands (I, II, III). Absorption bands I remain at positions (408−419 nm) similar to those of the Soret band of porphyrin monomers, bands II are observed at 550−560 nm, and bands III are exceedingly red-shifted at 850−1050 nm. Bands II become sharper as compared with those for the meso-β doubly linked diporphyrins **7**. The molecular extinction coefficients of

(26) Scheidt, W. R.; Mondal, J. U.; Eigenbrot, C. W.; Adler, A.; Radonovich, L. J.; Hoard, J. L. *Inorg. Chem.* **1986**, *25*, 795.

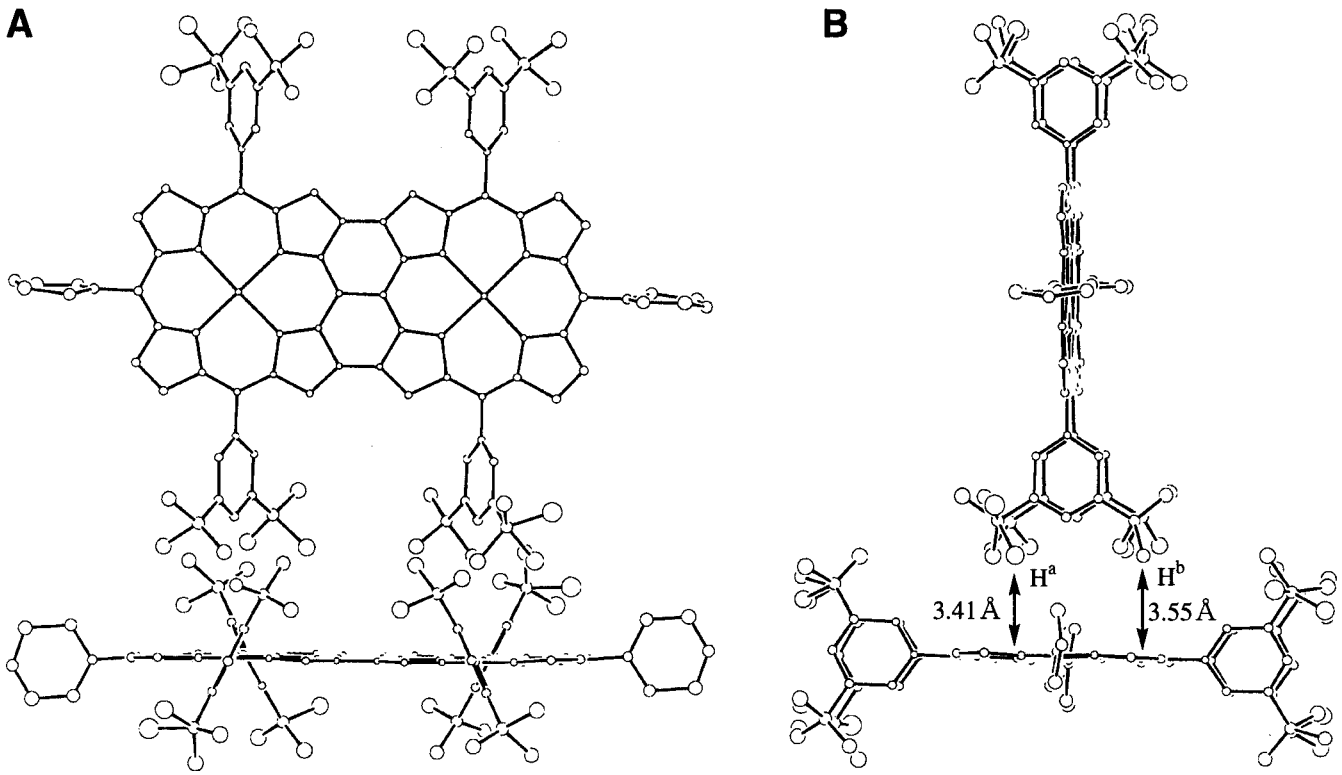

Figure 5. Molecular structures of **8g**. (A) Top view. (B) Side view. Hydrogen atoms have been omitted for clarity.

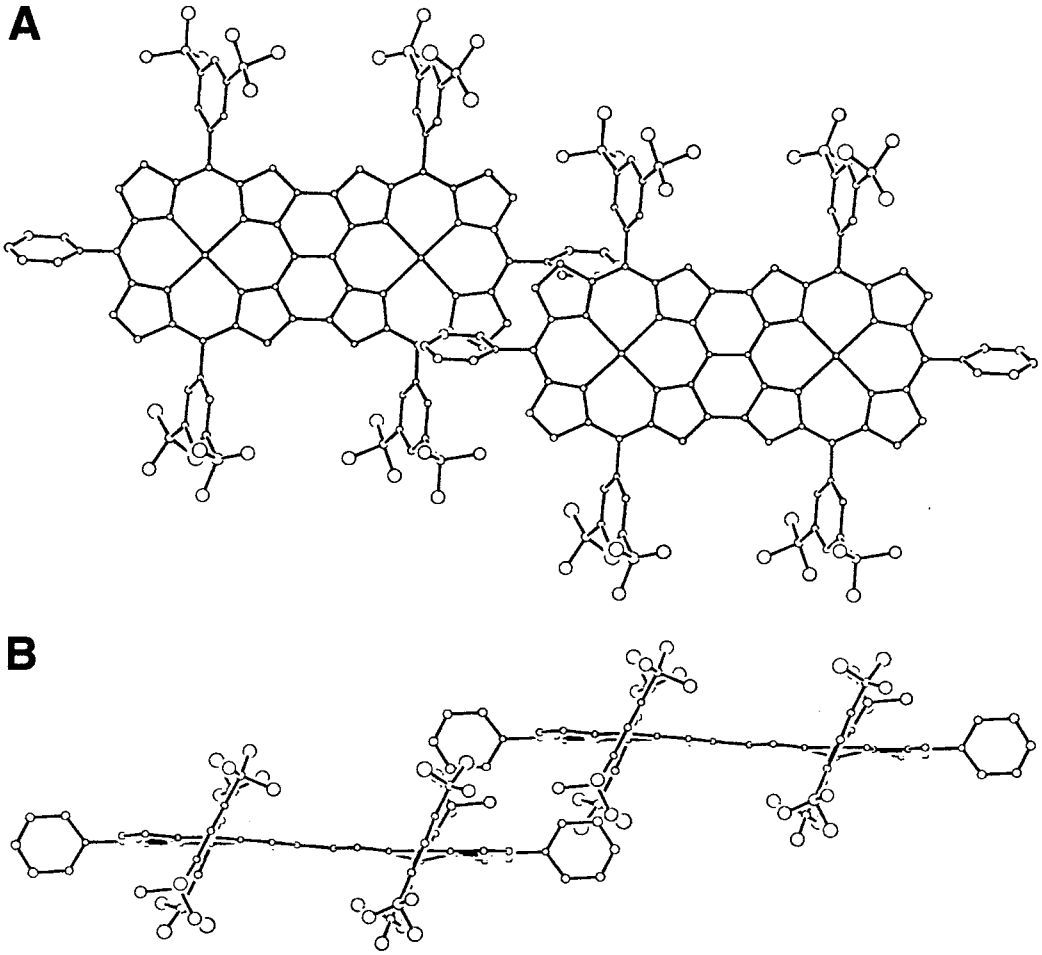

Figure 6. Molecular structures of **8j**. (A) Top view. (B) Side view. Hydrogen atoms have been omitted for clarity.

bands I in **8** are similar to those of **7** but the molecular extinction coefficients of bands II are larger in comparison to those in **7**. In the particular case of the Pd^{II}−diporphyrin **8f**, band II is higher than band I. Effects of the central metals upon the

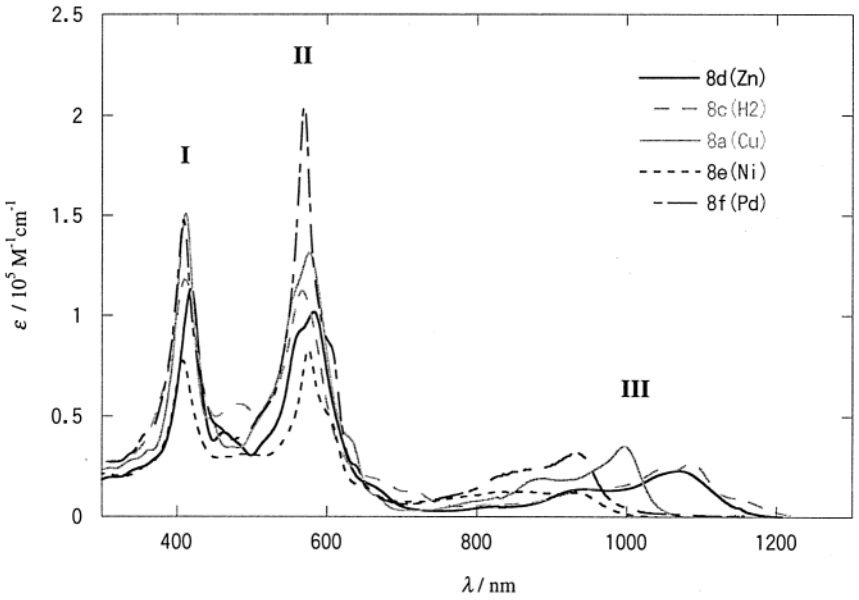

Figure 7. Absorption spectra of meso−meso $\beta-\beta$ $\beta-\beta$ triply linked diporphyrins in $CHCl_3$.

positions of bands III are similar to those found for **7**. Namely, the bathochromic shifts are modest for the Ni^{II}− and Pd^{II}− diporphyrins **8e** and **8f** and are large for the Zn^{II}− and free-base diporphyrin **8d** and **8c,** which exhibit the bands III at 1068 and 1086 nm, respectively.

Meso−Meso *β-β* Doubly Linked Diporphyrins 9. We have also examined the oxidative transformation of meso−meso singly linked Ni^{II}−diporphyrin **5a** to **8e**, since the cation radicals formed from Ni^{II}−porphyrins are known to favor A_{1u} HOMO. Curiously, the similar reaction of **5a** with BAHA afforded meso−meso $\beta-\beta$ doubly linked diporphyrin **9a** (chlorine free, 10%) and **9b** (monochlorinated, 20%) as the third type of fused diporphyrin in addition to triply linked diporphyrin **8e** (10%) and **8l** (monochlorinated, 20%). The doubly linked diporphyrin **9a** displayed a parent molecular ion peak at $m/z = 1862$ (calcd for $C_{124}H_{140}N_8Ni_2$, 1860) in its FAB-MS (or MALDI-TOF) mass spectrum and exhibited six doublets for the β-protons at 7.51, 8.48, 8.50 (for 4H), 8.51, and 8.53 ppm and a singlet for the β-protons adjacent to the $\beta-\beta$ connection at 8.84 ppm in its ^1H NMR spectrum. The electronic absorption spectrum of **9a** is similar to that of the meso-β doubly linked diporphyrin **7b**, exhibiting also three main bands $\lambda_{max} = 410$, 490, and 735 nm (Figure 8). The structure of the monochlorinated **9b** has been inferred by the analogy of its properties to those of **9a**; $m/z =$ 1891 (calcd for $C_{124}H_{139}N_8ClNi_2$, 1891; $\lambda_{max} = 407$, 492, and 728 nm).

The final structural determination of **9a** has come from its X-ray crystal structure (Figure 9). The two porphyrin rings take a nearly coplanar conformation but with large ruffling toward the opposite directions. The mean plane deviation is 0.34 Å, the Ni−Ni distance is 8.20 Å, and the mean Ni−N distance is 1.90 Å. As a result of the opposite ruffling, **9a** has a helical structure with nearly C_2 symmetry and the remaining two β-hydrogens adjacent to the meso−meso connection are fixed to be about 3.20 Å apart. In the crystal packing structure, **9a** is arranged like a slipped parallel sheet with pairing of chiral enantiomers.

The helical structure of **9a** has been confirmed by its separation into the two enatiomers by HPLC with a chiral preparative column. The isolated two enantiomers displayed opposite Cotton effects in the CD spectra (Figure 8). In the CD spectrum of the first eluting isomer, **9a(A)**, the first Cotton effect

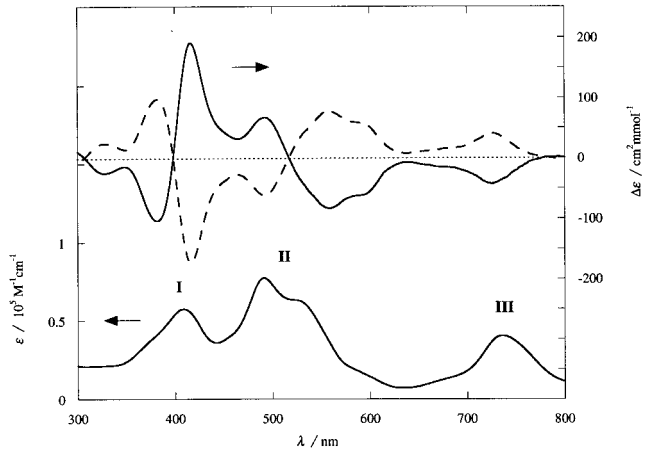

Figure 8. Bottom, absorption spectrum of **9a**. Top, CD spectra of **9a** in $CHCl_3$; the first eluting isomer **9a(A)** (—); the secondary eluting isomer **9a(B)** (- - -).

with the negative sense was observed around 700 nm, which corresponds to absorption band III. But the peak position in the CD spectrum was at 725 nm, being blue-shifted by 11 nm from absorption band III. The second and third ones were observed as bisignate split Cotton effects, both of which coincide very closely with absorption bands I and II seen in the absorption spectra. These bisignate two Cotton effects had the opposite sign, and the intensity of the CD effect at band I was distinctly stronger than that at band II. These CD spectra provide rich information on the absorption properties of the meso−meso $\beta-\beta$ doubly linked diporphyrins, which will be discussed below. The activation barrier for the interconversion between the two enantiomers has been determined by monitoring the CD intensity decrease at 416 nm with a toluene solution containing **9a** (1.04×10^{-2} mM) at 333−363 K. The racemization rate constants k_R that obey first-order kinetics have been determined at different temperatures (Supporting Information 4). The activation parameters obtained ($\Delta G^{\ddagger} = 111$ kJ mol^{-1}, $\Delta H^{\ddagger} = 101$ kJ mol^{-1}, $\Delta S^{\ddagger} = -30.4$ J mol^{-1} K^{-1}, $\Delta E = 104$ kJ mol^{-1}) are very similar to those determined for the pentahelicene ($\Delta G^{\ddagger} = 101$ kJ mol^{-1}, $\Delta H^{\ddagger} = 95.8$ kJ mol^{-1}, $\Delta S^{\ddagger} = -17.2$ J mol^{-1} K^{-1}, $\Delta E = 98.3$ kJ mol^{-1}) but distinctly smaller than those of the hexahelicene ($\Delta G^{\ddagger} = 146$ kJ mol^{-1}, $\Delta H^{\ddagger} = 152$ kJ mol^{-1}, $\Delta S^{\ddagger} = -17.6$ J

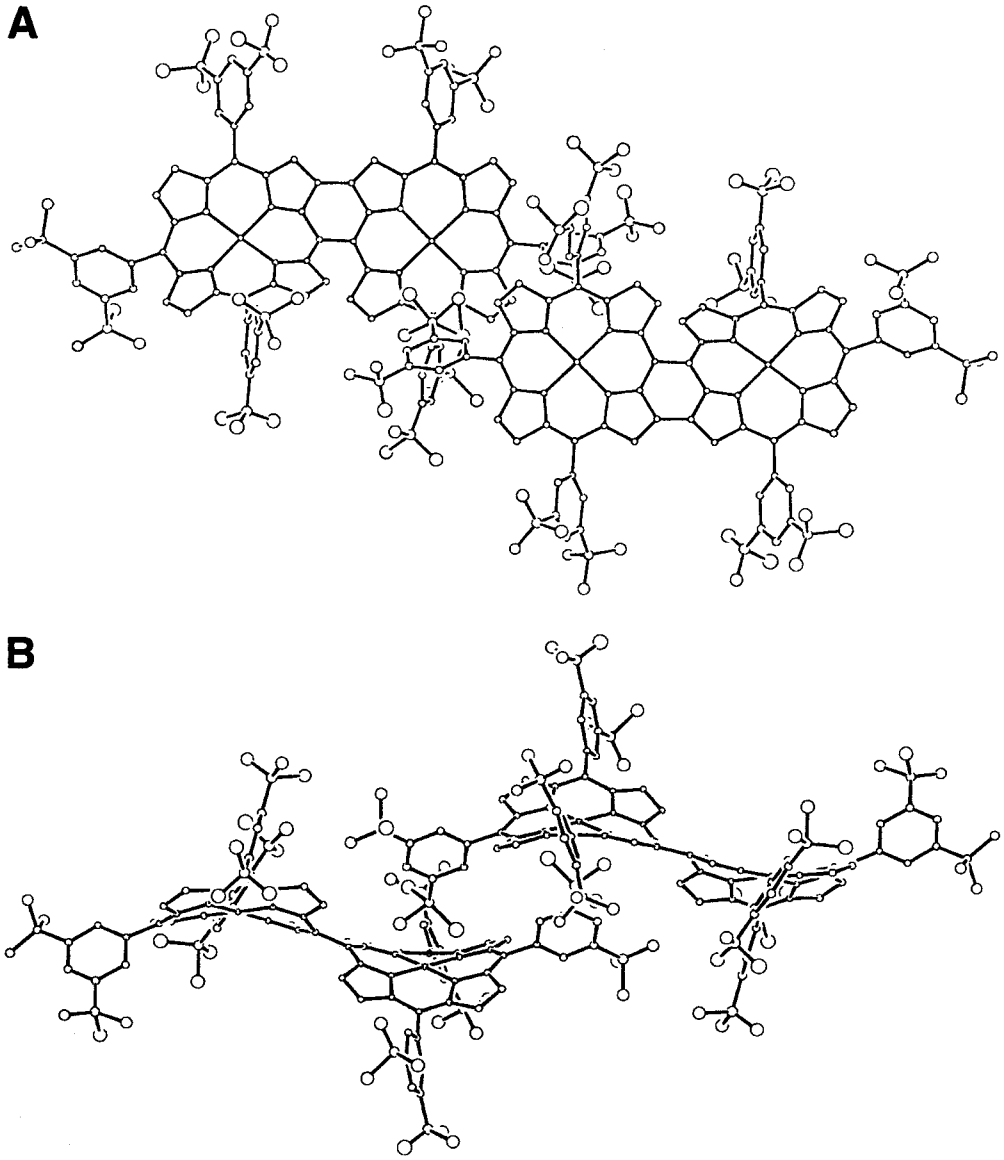

Figure 9. Molecular structures of **9a**. (A) Top view. (B) Side view. Hydrogen atoms have been omitted for clarity.

mol^{-1} K^{-1}, ΔE = 149 kJ mol^{-1}) and other higher ordered helicenes.[27]

Oxidation Reactions of Other Meso−Meso Singly Linked Diporphyrins. In contrast to the successful formation of the triply linked diporphyrin from the meso−meso linked Cu^{II}− and Ni^{II}−diporphyrins, neither free-base diporphyrin **5g**, Zn^{II}−diporphyrin **5h**, nor Pd^{II}−diporphyrin **5i** gave the triply linked diporphyrins under similar oxidation conditions. Diporphyrins **5g** and **5i** were almost recovered and **5h** was merely demetalated to **5g**.

^{1}H NMR Spectra. The chemical shifts of the peripheral β-protons and the inner NH protons provide important information on the aromaticity of the electronic π system of porphyrins. Figure 10 shows some representative chemical shifts of the free-base porphyrins and diporphyrins in $CDCl_3$. In **4i** and **4j**, the β-protons appear at 8.90−9.33 ppm and the inner NH protons appear at −2.90 and −2.66 ppm. In **5g**, the inner β-protons (H^a and H^b) and inner NH protons are upfield shifted to 8.10 and 8.61 ppm and −2.11 ppm, respectively, while the outer β-protons (H^c and H^d) remain at chemical shifts similar in comparison to those of the monomer. The observed upfield shifts of the inner β-protons indicate their location in the shielding region of the ring current of the perpendicularly arranged counterpart porphyrin. In contrast, the ^{1}H NMR spectrum of the meso-β doubly linked diporphyrin **7g** shows the upfield shifts of the outer β-protons (H^b, H^c, H^d, H^e) at 8.42−8.53 ppm and the downfield shifts of the inner β-protons (H^a, H^g) at 9.18 and 9.55 ppm relative to those in **4i** and **4j**. The downfield shifts of H^a and H^g may be ascribed due to the deshielding ring current effect of the other porphyrin, since they are positioned in the same plane with the other porphyrin ring, while the upfield shifts of the outer β-protons (H^b, H^c) suggest the decreased aromatic ring current probably associated with enhanced conjugation over the array. Such a tendency seems to be stronger in the spectrum of **8c** with distinct upfield shifts of the outer β-protons at 7.60−7.63 ppm. The inner NH protons are clearly downfield shifted in order of **4i** and **4j** < **5g** < **7g** < **8c**. The similar trends of the decreased ring current effect upon the increase of the π-conjugation were also suggested from the ^{1}H NMR spectra of the Ni^{II}− and Zn^{II}−diporphyrins (See Experimental Section).

Electrochemistry. The electrochemical properties, particularly the one-electron oxidation potentials, were studied by cyclic

(27) (a) Goediche, C.; Stegemeyer, H. *Tetrahedron Lett.* **1970**, *12*, 937. (b) Martin, R. H.; Marchant, M.-J. *Tetrahedron Lett.* **1972**, *35*, 937. (c) Martin. R. H.; Marchant. M-.J. *Tetrahedron* **1974**, *30*, 347.

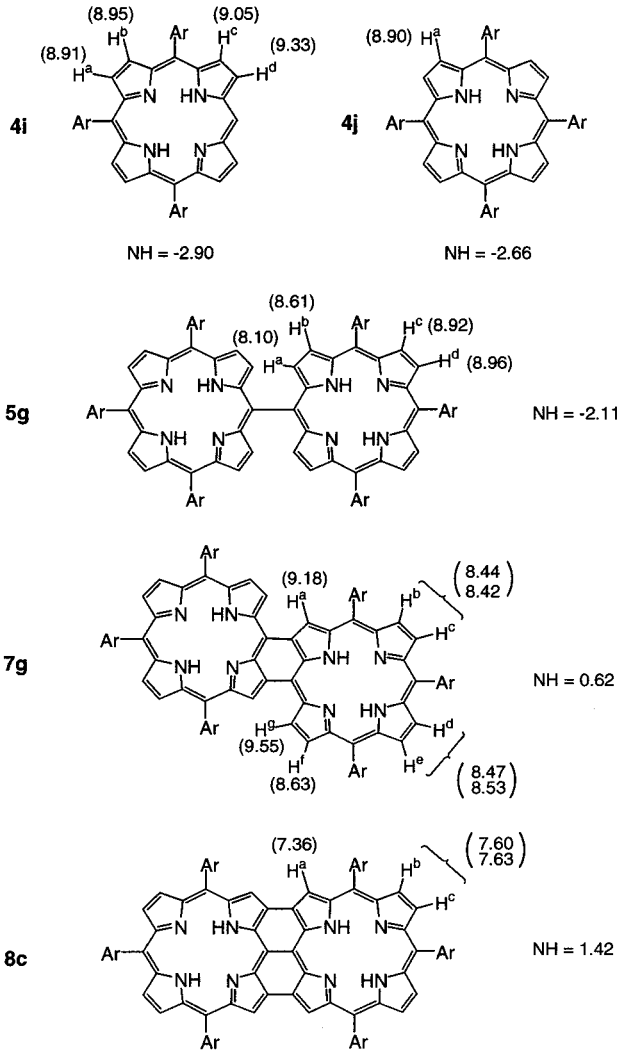

Figure 10. Representative ^{1}H NMR chemical shifts of free-base porphyrins **4i**, **4j**, **5g**, **7g**, and **8c**.

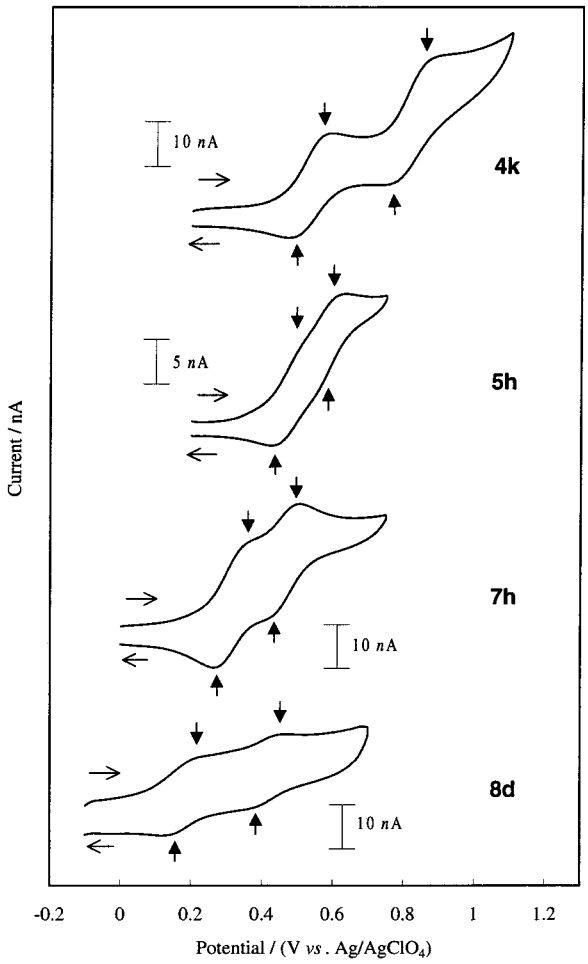

Figure 11. Cyclic voltammograms (E_{ox} (V) vs $AgClO_4/Ag$) for the oxidation of Zn^{II}−porphyrin **4k** and Zn^{II}−diporphyrins, **5h**, **7h**, and **8d** in $CHCl_3$. Scan rate, 30 mV/s; working electrode, Pt; supporting electrolyte, 0.1 M $Bu_4N{\cdot}BF_4$.

voltammetry in $CHCl_3$ containing 0.1 M tetrabutylammonium tetrafluoroborate ($Bu_4N{\cdot}BF_4$) as supporting electrolyte. Unfortunately, at the present stage, waves associated with electrochemical reduction could not be measured precisely in our hands. The cyclic voltammograms of the Zn^{II}−porphyrins, **4k**, **5h**, **7h**, and **8d**, are shown in Figure 11. The monomer **4k** underwent reversible first and second oxidations at 0.52 and 0.83 V versus $Ag/AgClO_4$, while the two reversible oxidation waves at 0.47 and 0.59 V in the meso−meso singly linked diporphyrin **5h** have been assigned as split first oxidation waves (one electron per porphyrin) as judged from the results of other electronically coupled diporphyrins.[2,4] Here we define the value of potential difference, $\Delta E = E_{OX1} - E_{OX2}$, where E_{OX1} and E_{OX2} represent split potentials for the first oxidation. E_{OX1} of **5h** was lowered with respect to that of **4k**, indicating the lift up of HOMO orbital in **5h**, while E_{OX2} was higher than that of **4k**, probably as an influence of the positive charge first generated. The one-electron oxidation potentials were detected at 0.31 and 0.47 V for **7h** and at 0.17 and 0.42 V for **8d**, respectively.

The oxidation potentials were also determined for Cu^{II}−, free-base, Ni^{II}−, and Pd^{II}−porphyrins, and the results are listed in Table 2.

These studies revealed that within the same metalated series the decrease of the first oxidation potential followed the same order of **4** > **5** > **7** > **8** as similar to the trend found for the Zn^{II}−diporphyrin series (Figure 12) and the increase of the ΔE values also followed the same order of **5** < **7** < **8.** The ΔE values were also a function of the central metal in the porphyrin core. A similar trend was found for the Pd^{II}−, Ni^{II}−, (free-base), and Cu^{II}−diporphyrin series, while a somewhat different trend was found for the Zn^{II}−diporphyrins. In the former group, the ΔE values of **5** were 0.18−0.21 V, those of **7** were 0.31−0.37 V, and those of **8** were 0.39−0.44 V, whereas in the Zn^{II}−diporphyrin series, the ΔE values were 0.13, 0.16, and 0.25 for **5h**, **7h**, and **8d**, respectively. The ΔE values of **7h** and **8d** were considerably smaller compared with those of the other diporphyrins.

Discussion

As described above, the unsubstituted peripheral side of 5,-15-diaryl- and 5,10,15-triarylmetalloporphyrins can be made reactive for the direct coupling upon treatment with BAHA. Taking advantage of this, we have developed the synthetic routes to the three novel fused diporphyrins **7**, **8**, and **9**. These three fused diporphyrins are forced to take nearly coplanar geometries, which cause extensive π conjugation over the diporphyrins. In the synthesis of **7**, the use of Ni^{II}− or Pd^{II}−porphyrins is recommended because of their highly regioselective initial meso-β coupling arising from their A_{1u} HOMO orbitals, although meso-β doubly linked Pd^{II}−diporphyrin has been

Table 2. Oxidation Potentials of **4**, **5**, **7**, **8** and **9** in $CHCl_3$[a]

	Zn				Cu				H_2				Ni				Pd		
	E_{OX1}	E_{OX2}	ΔE		E_{OX1}	E_{OX2}	ΔE		E_{OX1}	E_{OX2}	ΔE		E_{OX1}	E_{OX2}	ΔE		E_{OX1}	E_{OX2}	ΔE
4k	0.52			**4e**	0.72			**4i**	0.75			**4b**	0.76			**4g**	0.82		
5h	0.47	0.59	0.13	**5c**	0.68	0.86	0.18	**5g**	0.71	0.88	0.17	**5a**	0.73	0.91	0.18	**5i**	0.79	1.01	0.21
7h	0.31	0.47	0.16	**7c**	0.47	0.78	0.31	**7g**	0.46	0.79	0.33	**7b**	0.52	0.84	0.32	**7d**	0.57	0.94	0.37
												9a	0.48	0.87	0.39				
8d	0.17	0.42	0.25	**8a**	0.39	0.78	0.39	**8c**	0.35	0.75	0.40	**8e**	0.46	0.87	0.41	**8f**	0.51	0.95	0.44

[a] E_{OX1}, first oxidation potential (V); E_{OX2}, second oxidation potential (V); $\Delta E = E_{OX2} - E_{OX1}$.

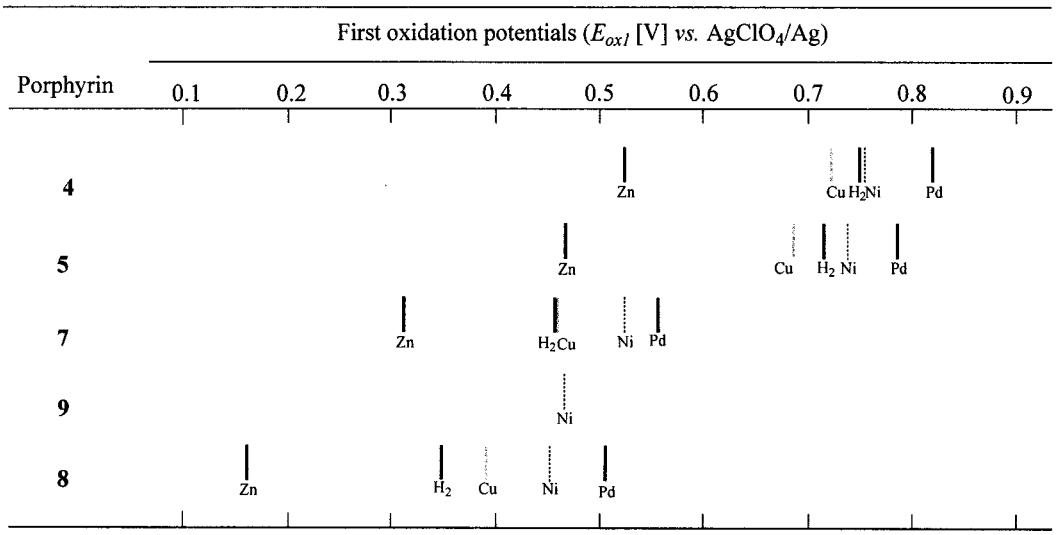

Figure 12. Comparison of E_{OX1} (V) vs $AgClO_4/Ag$ in $CHCl_3$.

shown more prone to peripheral β chlorination. This is in contrast to the successful synthesis of meso−meso singly linked diporphyrin and higher porphyrin arrays from the corresponding Zn^{II}−porphyrins which seem to have A_{2u} HOMO orbital.[15] In the oxidative transformation of the meso−meso singly linked diporphyrin to the meso−meso $\beta-\beta$ $\beta-\beta$ triply linked diporphyrins, the Cu^{II}−diporphyrin substrates such as **5c** and **5f** are of preferable choice, in that they give triply linked diporphyrins in good yields without noticeable demetalation during the oxidation with BAHA and are quantitatively demetalated to the corresponding free-base diporphyrins, from which a variety of metalated triply linked diporphyrin can be prepared.

In the course of this study, we noted several interesting reactivities of the metal porphyrins under the present oxidation conditions. First, in the transformation of **5c** to **8a**, we found that the peripheral β chlorination was fairly suppressed in C_6F_6. The results in C_6H_6 and $CF_3C_6H_5$ (Table 1, entries 6 and 7) suggested that the chlorine atom abstraction was taking place from BAHA. Thus, the observed suppression of the peripheral β chlorination in C_6F_6 can be attributed to suppression of the reaction of **8a** with BAHA, while **8a** is very susceptible to the peripheral chlorination due to its high HOMO energy in comparison to **5c**. Here it is interesting to note that the solubility of **8a** is quite poor, almost insoluble in C_6F_6, but certainly soluble in $CHCl_3$, C_6H_6, and $CF_3C_6H_5$. The starting substrate **5c** is much soluble in C_6F_6. It is therefore conceivable that, during the reaction in C_6F_6, the oxidation product **8a** once formed may be precipitated out from the reaction mixture, thereby escaping from the undesirable reaction with BAHA. In line with this consideration, the formation of turbid material was indeed observed in the reaction of **5c** with BAHA in C_6F_6.

The second interesting reactivity is that the meso−meso $\beta-\beta$ doubly linked diporphyrin **9** was isolated only in the reaction of Ni^{II}−diporphyrin **5a**. The similar meso−meso $\beta-\beta$ doubly linked diporphyrin product was never detected in the reaction of the Cu^{II}−porphyrins **5c** and **5f**. Accumulation of **9** may be rationalized in terms of its constrained helical structure in which the two β-hydrogens adjacent to the meso−meso linkage are kept apart from the coupling distance. This may be brought about by the large ruffling of the porphyrin core which is characteristic of Ni^{II}−porphyrins.[24] By contrast, Cu^{II}−porphyrins usually tend to take more planar structures.[25,28] If the similar planar structure is favored also for the meso−meso $\beta-\beta$ doubly linked Cu^{II}−diporphyrin, the two β-hydrogens adjacent to the meso−meso connection would be located closer, hence facilitating subsequent $\beta-\beta$ coupling to complete the triple linkage.

Fortunately, we have obtained X-ray quality single crystals for the three types of fused diporphyrins, meso-β doubly linked Ni^{II}−diporphyrin **7b** and Cu^{II}−diporphyrin **7c**, meso−meso $\beta-\beta$ $\beta-\beta$ triply linked Cu^{II}−diporphyrin **8g** and Zn^{II}−diporphyrin **8j**, and meso−meso $\beta-\beta$ doubly linked Ni^{II}−diporphyrin **9a**. In most cases, the structural parameters including bond lengths, bond angles, mean plane deviations, and mean metal−nitrogen distances that relate with porphyrin ring distortion are quite similar to those of the reference Ni^{II}−, Cu^{II}−, and Zn^{II}−TPP, respectively (Supporting Information 5). Therefore, it may be concluded that the fused connection scarcely alters the basic skeletons of the each porphyrin ring but serves to force coplanar arrangements of the diporphyrins.

The doubly linked diporphyrins **7b**, **7c**, and **9a** show ruffling depending on the linkage pattern and the coordinated metal, whereas the triply linked diporphyrins **8g** and **8j** display more planar geometries. The ruffling for the Ni^{II}−diporphyrins **7b**

(28) Cu^{II}−TPP was reported to take a ruffled structure with a mean plane deviation of 0.205 Å (ref 25), but we found that 5,15-bis(3,5-dioctyloxy)-phenyl Cu^{II}−porphyrin was more planar with a mean plane deviation of 0.014 Å and a mean Cu−N distance of 1.99 Å: Aratani, N.; Yoshida, N.; Osuka, A., unpublished results.

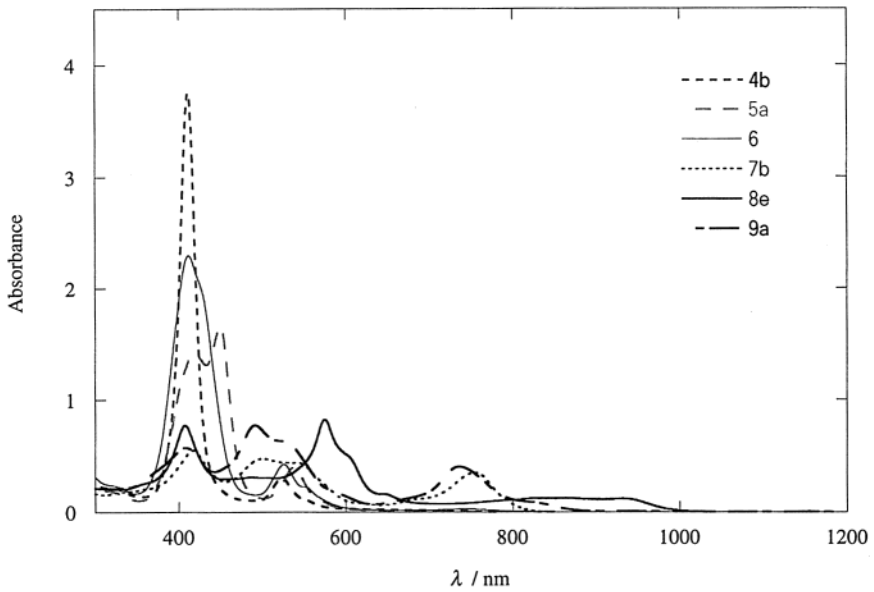

Figure 13. Absorption spectra of Ni^{II}−porphyrin series including **4b**, **5a**, **6**, **7b**, **8e**, and **9a** in $CHCl_3$. Concentrations are 2×10^{-6} M for **4b** and 1×10^{-6} M for the other diporphyrins.

and **9a** may be ascribed largely to a smaller size of the Ni^{II} cation toward the central porphyrin cavity.[24] In line with this interpretation, the average Ni−N distances (1.92 and 1.90 Å for **7b** and **9a**) are similar to the reported 1.929 Å for Ni^{II}−TPP.[24] In **9a**, the steric congestion between the remaining peripheral β-hydrogens adjacent to the meso−meso bond causes additional distortion. Compared with Ni^{II}−porphyrins, Cu^{II}−porphyrins have been known to take more planar structures.[25,28] Thus, the ruffled structure of **7c** suggests some intrinsic distortion arising from the meso-β double linkage, while such distortion would be smaller in triply linked diporphyrins, judging from more planar structure of **8g**. Another interesting observation is the orthogonal crystal packing of **8g** and **8k**, which suggests attractive CH−π interaction between the 3,5-di-*tert*-butylphenyl groups and diporphyrin π system.[29] The distances between the carbon atoms of the *tert*-butyl group and the porphyrin plane are 3.41 and 3.55 Å, in the reported range of CH−π interaction.[29] This interaction may be enhanced by the large polarizability of the triply linked diporphyrins associated with their wide π-electronic system. On the other hand, **8j** shows not orthogonal but parallel packing with large offset. This may be ascribed to ethanol coordination to the zinc ion.

All of the diporphyrin set is available only for Ni^{II}−porphyrins, and thus, their absorption spectra are compared in Figure 13. In contrast to the sharp Soret band of the monomer **4b**, the singly linked diporphyrins **5a** and **6** exhibit perturbed Soret bands but the spectral changes in the Q-bands are rather modest despite the direct connections. As seen for the corresponding Zn^{II}−diporphyrins,[17] the Soret band of **5a** is split at 419 and 450 nm, and that of **6** is observed as a broad band with a peak at 412 nm with a shoulder at 425 nm, and the Q-bands are observed at 523, 538, and 526 nm for **4b**, **5a**, and **6**, respectively. The relatively small spectral changes may be ascribed to their almost perpendicular conformations. The spectral changes in **5a** and **6** can be qualitatively understood in terms of the exciton coupling between the transition dipole moments of the porphyrin, which depends on the oscillator strength, and the relative geometry of the interacting transition dipole moments. In the case of the Zn^{II}−diporphyrins, the exciton coupling energies in the Soret band region were evaluated to be 4250 and 2530 cm^{-1}, respectively, for the meso−meso linked and meso-β linked diporphyrins on the basis of the deconvolution of the split Soret bands.[17] Analogously, the exciton coupling energies have been evaluated to be 3300 and 2050 cm^{-1} for **5a** and **6**, respectively. Smaller exciton coupling energies in the Ni^{II}−porphyrins arise from the smaller oscillator strength of the Ni^{II}−porphyrin monomer compared with that in the Zn^{II}−porphyrin monomer, and the different values for **5a** and **6** can be ascribed to the different geometries. From this analysis it may be concluded that there is large electronic interaction between the two porphyrin in **5a** and **6** but they are *not conjugated*.

In contrast, the electronic π systems in the fused diporphyrins **7b**, **8e**, and **9a** can be regarded *conjugated*, judging from their entirely perturbed absorption spectra. Evidently, the forced coplanar geometries of the fused diporphyrins allow the π conjugation. The absorption spectra of the doubly linked diporphyrins **7b** and **9a** are similar to each other, and the triply linked diporphyrin **8e** displays the most altered absorption spectrum with the largest splitting of the Soret-like band and extension of its Q-band into far-infrared region.

The absorption spectral pattern consisting of the three main bands (I, II, III) is common for all the fused diporphyrins. Although the assignment of these bands has not been fixed yet, it may be possible to qualitatively understand these spectral characteristics on the basis of the well-established Gouterman four-orbital theoretical model for the absorption spectra of porphyrins.[30] In the four-orbital theory, the B- and Q-bands both arise from $\pi-\pi^*$ transitions and can be explained in terms of a linear combination of transitions from a_{1u} and a_{2u} HOMO orbitals to a degenerate pair of e_{gx} and e_{gy} LUMO orbitals. The two HOMO orbitals happen to have the same energy and the configurational interaction results in two bands with very different intensities and wavelengths; the intense short-wavelength B-band and the weak long-wavelength Q-band. On the other hand, the fused connection causes a significant perturbation that breaks down the degeneracy of the e_{gx} and e_{gy}

(29) (a) Aurivillius, B.; Carter, R. E. *J. Chem. Soc., Perkin 2* **1978**, 1033. (b) Nishino, M.; Hirota, M. *Tetrahedron* **1989**, *45*, 7201.

(30) (a) Gouterman, M. *J. Mol. Spectrosc.* **1961**, *6*, 138. (b) Bilsel, O.; Rodriguez, J.; Milam, S. N.; Gorlin, P. A.; Girolami, G. S.; Suslick, K. S.; Holten, D. *J. Am. Chem. Soc.* **1992**, *114*, 6528.

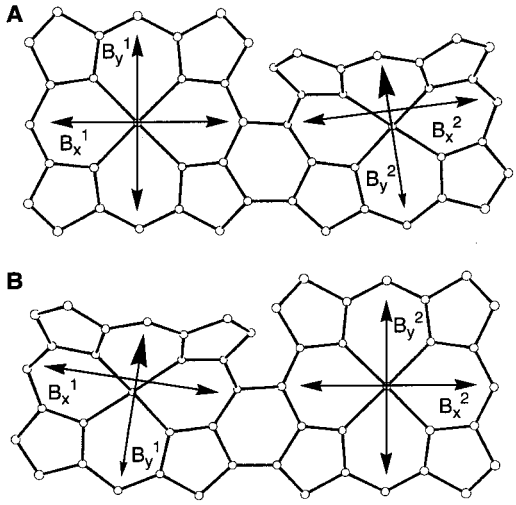

Figure 14. Transition dipole moment arrangements in **9a**.

orbitals. It may be pertinent to assign bands I and II to the allowed Soret-like transitions along the shorter and longer molecular axes of the diporphyrins, respectively, while band III may be assigned to a formally forbidden Q-bandlike transition in the D_4 symmetry Zn^{II}−porphyrin monomer. Therefore, the enhancement of bands III in the fused diporphyrins can be understood in terms of symmetry lowering. The CD spectra of the enationmers **9a(A)** and **9a(B)** are quite informative on the absorption characteristics. Consideration of the two transition dipole moments, B_x and B_y, respectively, nearly parallel and perpendicular to the long molecular axis of the diporphyrin as shown in Figure 14 can explain the perturbed absorption spectra and CD Cotton effects through the excitonic interactions of the resultant four transition dipole moments. The coupling of the two B_y transition dipole moments does not lead to the substantial spectral change nor spectral shift because of their almost perpendicular arrangement but gives rise to the strong bisignate Cotton effect at the absorption band I position, since the two B_y transition dipole moments are held at a chiral perpendicular arrangement. On the other hand, the coupling between the nearly parallel two B_x transition dipole moments leads to a dipole-allowed red-shifted transition that corresponds to the band II and almost dipole-prohibited blue-shifted transition which cannot be detected clearly. The coupling of the B_x dipole moments also brings about the bisignate CD signal at the band II region, but its sign is opposite to the CD effect of band I and its intensity is weaker because of the unfavorable arrangement of the two B_x for the Cotton effects. According to the empirical chirality exciton methods and the related studies on the helical molecules, the first-eluting isomer **9a(A)** that exhibits the split CD Cotton effects of positive chirality at band I and those of negative chirality at band II can be assigned to the counterclockwise-skew structure A shown in Figure 14, and the secondary-eluting isomer **9a(B)** that exhibits the split CD Cotton effects of the opposite sense can be assigned to the clockwise-skew structure B.[31] These interpretations seem to help us to understand the absorption spectra of the triply linked diporphyrins **8**, in which two B_x transition dipole moments are completely in a line along the meso−meso bond, thereby giving rise to sharper and intensified bands II, as seen in the absorption spectrum of **8f**.

As described above, the oxidation potentials of the singly and doubly linked diporphyrins exhibit systematic changes upon the structural changes and the central metals. The first question may be the site of oxidation, i.e., the metal or the ligand. Although we do not have definitive evidence for it, the voltammetric behaviors of the present Zn, Cu, H_2, Ni, and Pd diporphyrins as a group are remarkably similar, thus suggesting electron removal is commonly occurring from the diporphyrin ligand but not from the metal center. The dependence of oxidation potentials of the meso−meso linked and fused diporphyrins on the identity of the central metal follows that seen in 5,10,15-triaryl-substituted porphyrin monomer, becoming harder in the order of Zn, Cu, H_2, Ni, and Pd, probably reflecting the electronegativity of the metals. Judging from the Ni^{II}−porphyrin series, the electronic interaction of the meso−meso $\beta-\beta$ doubly linked diporphyrins **9** may be placed between **7** and **8**. Within the same metalated diporphyrin series, the first oxidation potentials decrease in the order of **4** > **5** > **7** ≥ **9** > **8**, suggesting the lift-up of the HOMO orbital in this order. The ΔE values were also found to increase in the reversed order of **5** < **7** ≤ **9** < **8**, probably reflecting the increasing delocalized nature of one-electron oxidized diporphyrins. It is interesting to note that the ΔE values are also a function of the central metals. There is a distinct difference between the Zn^{II} series and the other diporphyrin series, which, we believe, may be derived from a difference in the favored HOMO orbital characteristics of the porphyrin monomer unit, since only the Zn^{II}−porphyrin favors A_{2u} HOMO.

Inspection of the ^{1}H NMR chemical shifts shown in Figure 10 has revealed that the shielding and deshielding effects of porphyrin ring currents are weakened upon increasing connection between the two units, since the outer β-protons are shifted to high field and the inner NHs are shifted to downfield in the order of **4i** and **4j** < **5g** < **7g** < **8c**. Similar results have recently been reported by Smith et al. for the directly fused porphyrin trimers that bear the same connection as that of **3**.[11] Taken together, the reduced ring current may be ascribed to the increased conjugation over the π network of the diporphyrins. But, as discussed above, the structural parameters of the porphyrin cores are scarcely affected by direct fused connection. Therefore, it may be concluded that the fused connection only serves to provide the coplanar π network without affecting the porphyrin cores to a significant extent, particularly in the case of **8**.

Collectively, the electronic absorption spectra, the first one-electron potential, the splitting of the first one-electron oxidation potential, and the ^{1}H NMR spectra indicated the increase of the electronic interaction between the two porphyrins in the order of **5** < **7** ≤ **9** < **8**. Judging from these properties, the triply linked diporphyrins **8** have been concluded to exert the strongest electronic interactions and the smallest optical HOMO−LUMO gaps (1.14−1.33 eV) among the fused diporphyrins studied so far.[8−12] In addition, the triply linked diporphyrins **8** have the highly symmetric structure and are likely to be free from severe structural distortion. Therefore, extension of this synthetic strategy to higher oligomeric and polymeric porphyrin arrays will be a fascinating next project.[32]

Experimental Section

General Information. All reagents and solvents were of the commercial reagent grade and were used without further purification

(31) (a) Nakanishi, K.; Berova, N. In *Circular Dichroism: Pronciples and Applications*; Nakanish, K., Berova, N., Woody, R. W., Eds.: VCH Publishers Inc.: NewYork, 1994; p 361. (b) Mason, S. F. *Molecular Optical Activity and the Chiral Discriminations*; Cambridge University Press: Cambridge, U.K., 1982. (c) Harada, N.; Nakanishi, K. *Acc. Chem. Res.* **1972**, *5*, 257.

(32) Recently we found meso−meso linked diporphyrin **5h** can be converted to **8d** by oxidation with 2,3-dichloro-5,6-dicyano-1,4-benzoquinone (DDQ) in the presence of $Sc^{III}(OTf)_3$, and this method was applicable to longer arrays: Tsuda, A.; Osuka, A. *Science* **2001**, *293*, 79.

except where noted. Dry CH_2Cl_2, $CHCl_3$, and acetonitrile were obtained by heating under reflux and distillation over CaH_2. Solvents used for spectroscopic measurements were all spectroscopic grade. Preparative separations were performed by silica gel gravity flow column chromatography (Wakogel C-400), silica gel flash column chromatography (Merck Kieselgel 60H Art. 7736), and size exclusion gel permeation chromatography (Bio-Rad Bio-Beads S-XI, packed with toluene or $CHCl_3$ in a 4.5 × 95 cm gravity flow column; flow rate, 3.8 mL min^{-1}). Separation of the chiral isomers was performed by preparative HPLC with Sumichiral OA3100 preparative column (eluent, hexane:$CHCl_3$ = 97:3; flow rate, 1.2 mL min^{-1}; detected at 400−700 nm) and with a Jasco HPLC apparatus with a multiwavelength detector SHIMADZU SPD-M10A. ^{1}H NMR spectra were recorded in a $CDCl_3$ solution on a JEOL Alpha-500 spectrometer (operating at 500 MHz), and chemical shifts were represented as δ values in ppm relative to the internal standard of $CHCl_3$ (δ = 7.260 ppm). FAB mass spectra were recorded on a JEOL HX-110 spectrometer with the positive-FAB ionization method (accelerating voltage, 10 kV; primary ion sources, Xe) and 3-nitrobenzyl alcohol matrix, and high-resolution mass spectra (HRMS) were taken with CsI clusters as reference. MALDI-TOF mass spectra were recorded on a Kratos PC-Kompact Shimadzu MALDI 4 spectrometer using a positive-MALDI-TOF method with/without a sinapinic acid matrix. UV/visible/NIR absorption spectra were recorded on a Simadzu UV-3100PC UV/visible/NIR scanning spectrophotometer in a range of 200 and 2000 nm. CD spectra were recorded on a Jasco J-720WI spectrometer. Redox potentials were measured by the cyclic voltammetry method and differential pulse voltammetry method on a ALS electrochemical analyzer model 660. X-ray crystallography was performed on a Rigaku-Raxis imaging plate system.

General Procedure for Porphyrin Metalation. For Zn^{II} metalation, a saturated solution of $Zn(OAc)_2$ in MeOH was added to a solution of free-base porphyrin in $CHCl_3$, and the resulting mixture was refluxed for 1−2 h. For Ni^{II} metalation, a solution of free-base porphyrin in toluene was refluxed with $Ni(acac)_2$ for 5−6 h in the dark. For Cu^{II} metalation, a saturated solution of $Cu(OAc)_2$ in MeOH was added to a solution of free-base porphyrin in $CHCl_3$, and the resulting mixture was refluxed for 1−2 h in the dark. For Pd^{II} metalation, a solution of free-base porphyrin in $CHCl_3$ was stirred in the presence of $Pd(OAc)_2$ powder at room temperature for 2 days in the dark. After the complete metalation was confirmed by TLC and UV analyses, the mixture was poured into water, and the porphyrin products were extracted with $CHCl_3$. The organic layer was separated, and the combined extracts were washed with water and brine and dried over anhydrous Na_2SO_4. Finally, column chromatography over a silica gel column gave the respective pure metalated porphyrins.

Porphyrin Syntheses. All the porphyrin monomers were prepared according to the published methods.[15,33] Meso−meso singly linked diporphyrins were prepared by the metalation of the corresponding free-base diporphyrins, which were prepared by demetalation of meso−meso linked Zn^{II}−diporphyrins.[15]

Meso-β Doubly Linked Ni^{II}−Diporphyrin 7a. A 50-mL round-bottom flask was charged with a solution of **4a** (55 mg, 74 μmol) in $CHCl_3$ (20 mL). The reaction vessel was covered with foil. BAHA (73 mg, 89 μmol) was added in one portion, and the resulting mixture was stirred for 10 h at room temperature. The mixture was diluted with water, and the organic layer was separated off, washed with water, and dried over anhydrous $MgSO_4$. The products were initially separated by preparative SEC with $CHCl_3$ as an eluant, giving porphyrin pentamer (MALDI-TOF MS *m*/*z* = 3709 and 3741, UV/visible ($CHCl_3$) λ_{max} = 408, 559, 777, 899, and 1151 nm) as the first fraction, porphyrin tetramer (MALDI-TOF MS *m*/*z* = 2968, 3000 and 3032, UV/visible ($CHCl_3$), λ_{max} = 407, 559, 776, 910, and 1151 nm) as the second fraction, porphyrin trimer (MALDI-TOF MS *m*/*z* = 2229, 2260 and 2295, UV/visible ($CHCl_3$) λ_{max} = 405, 555, 765, 899, and 1151 nm) as the third fraction, and porphyrin dimer as the fourth fraction. The final fraction was recrystallized with $CHCl_3$ and MeOH to give **7a** (7 mg, 11%). Further characterization of the higher oligomeric porphyrins was abandoned due to their extremely poor solubilities, contamination of inseparable chlorinated products, and possible existence of inseparable syn−anti isomers. **7a**: mp >300 °C; ^{1}H NMR ($CDCl_3$) δ 1.52 (s, 36H, *t*-Bu), 1.54 (s, 36H, *t*-Bu), 7.74 (t, *J* = 1.8 Hz, 2H, Ar-H), 7.77 (t, *J* = 1.8 Hz, 2H, Ar-H), 7.80 (d, *J* = 1.8 Hz, 4H, Ar-H), 7.92 (d, *J* = 1.8 Hz, 4H, Ar-H), 8.41 (d, *J* = 4.9 Hz, 2H, Por-β), 8.46 (d, *J* = 4.9 Hz, 2H, Por-β), 8.73 (d, *J* = 4.9 Hz, 2H, Por-β), 8.98 (s, 2H, Por-β), 9.08 (d, *J* = 4.9 Hz, 2H, Por-β), 9.11 (d, *J* = 4.9 Hz, 2H, Por-β), and 9.42 (d, *J* = 4.9 Hz, 2H, Por-β); HRMS (FAB) found *m*/*z* 1548.59(2), calcd for $C_{96}H_{98}Cl_2N_8Ni_2$, *m*/*z* 1548.5998; UV/visible ($CHCl_3$) λ_{max} (ϵ) = 418 (55 400), 500 (46 200), and 756 (36 200) nm.

Meso-β Doubly Linked Ni^{II}−Diporphyrin 7a. A 50-mL round-bottled flask was charged with a solution of **4d** (10 mg, 13 μmol) in $CHCl_3$ (20 mL). The reaction vessel was covered with foil. BAHA (12 mg, 15 μmol) was added in one portion, and the resulting mixture was stirred for 10 h at room temperature. The mixture was diluted with water, and the organic layer was separated off, washed with water, and dried over anhydrous $MgSO_4$. The products were initially separated by preparative SEC with $CHCl_3$ as an eluant. The first eluting fraction was diporphyrin, and the second slowly eluting fraction was monomeric porphyrins. The first fraction was further separated by flash chromatography over a silica gel (Wakogel FC40) column (hexane/CH_2Cl_2 (95:5)) to give **5b** (1 mg, 10%) as the first fraction and **7a** (7 mg, 70%) as the second fraction.

Meso-β Doubly Linked Ni^{II}−Diporphyrin 7b. Porphyrin **4b** (30 mg, 32 μmol) was oxidized with BAHA (32 mg, 39 μmol) in 20 mL of $CHCl_3$ for 12 h at room temperature. The products were separated into diporphyrin and monoporphyrin fractions by SEC. The latter was identified as a 1:1 mixture of meso-chlorinated and meso-brominated porphyrins (**4c**, 9 mg, 28%). The former was further separated by flash chromatography over a silica gel (Wakogel FC40) column (hexane/CH_2Cl_2 (95:5)) to give **5a** (3 mg, 10%) as the first fraction and **7b** (16 mg, 53%) as the second fraction. **7b**: mp >300 °C; ^{1}H NMR ($CDCl_3$) δ 1.45 (s, 36H, t-Bu), 1.51 (s, 36H, *t*-Bu), 1.54 (s, 36H, *t*-Bu), 7.67 (t, *J* = 1.8 Hz, 2H, Ar-H), 7.72 (t, *J* = 1.8 Hz, 2H, Ar-H), 7.75 (t, *J* = 1.8 Hz, 2H, Ar-H), 7.79 (d, *J* = 1.8 Hz, 4H, Ar-H), 7.84 (d, *J* = 1.8 Hz, 4H, Ar-H), 7.96 (d, *J* = 1.8 Hz, 4H, Ar-H), 8.37 (d, *J* = 4.9 Hz, 2H, Por-β), 8.40 (s, 4H, 8.46, Por-β), 8.45 (d, *J* = 4.9 Hz, 2H, Por-β), 8.77 (d, *J* = 4.9 Hz, 2H, Por-β), 9.05 (s, 2H, Por-β), and 9.49 (d, *J* = 4.9 Hz, 2H, Por-β); HRMS (FAB) found *m*/*z* 1856.96(3), calcd for $C_{124}H_{140}N_8Ni_2$, *m*/*z* 1856.9908; UV/visible ($CHCl_3$) λ_{max} (ϵ) = 417 (55 100), 501 (47 600), 538 (43 900), and 756 (35 000) nm.

Meso-β Doubly Linked Cu^{II}−Diporphyrin 7c. Porphyrin **4e** (12 mg, 13 μmol) was oxidized with BAHA (13 mg, 15 μmol) in 10 mL of $CHCl_3$ for 12 h at room temperature. The products were separated into diporphyrin and monoporphyrin fractions by SEC. The latter was identified as meso-chlorinated porphyrin **4f** (3 mg, 24%). The former was further separated by flash chromatography over a silica gel (Wakogel FC40) column (hexane/CH_2Cl_2 (95:5)) to give **5c** (4 mg, 33%) as the first fraction and **7c** (3 mg, 25%) as the second fraction. **7c**: mp >300 °C; HRMS (FAB) found *m*/*z* 1866.99(2), calcd for $C_{124}H_{140}N_8Cu_2$, *m*/*z* 1866.9993; UV/visible ($CHCl_3$) λ_{max} (ϵ) = 419 (130 600), 551 (99 300), and 781 (76 300) nm.

Meso-β Doubly Linked Pd^{II}−Diporphyrins 7d, 7e, and 7f. Porphyrin **4g** (10 mg, 10 μmol) was oxidized with BAHA (10 mg, 12 μmol) in 10 mL of $CHCl_3$ for 12 h at room temperature. The products were separated into diporphyrin and monoporphyrin fractions by SEC. The former was further separated by flash chromatography over a silica gel (Wakogel FC40) column (hexane/CH_2Cl_2 (95:5)) to give **7f** (2 mg, 19%) as the first fraction, **7e** (2 mg, 20%) as the second fraction, and **7d** (2 mg, 20%) as the third fraction. **7d**: mp >205−208 °C; ^{1}H NMR ($CDCl_3$) δ 1.50 (s, 36H, *t*-Bu), 1.56 (s, 36H, *t*-Bu), 1.60 (s, 36H, *t*-Bu), 7.73 (t, *J* = 1.8 Hz, 2H, Ar-H), 7.79 (t, *J* = 1.8 Hz, 2H, Ar-H), 7.83 (t, *J* = 1.8 Hz, 2H, Ar-H), 7.92 (d, *J* = 1.8 Hz, 4H, Ar-H), 8.00 (d, *J* = 1.8 Hz, 4H, Ar-H), 8.14 (d, *J* = 1.8 Hz, 4H, Ar-H), 8.47 (d, *J* = 4.9 Hz, 4H, Por-β), 8.51 (d, *J* = 4.9 Hz, 2H, Por-β), 8.58 (d, *J* = 4.9 Hz, 2H, Por-β), 8.76 (d, *J* = 4.9 Hz, 2H, Por-β), 9.31 (s, 2H, Por-β), and 9.73 (d, *J* = 4.9 Hz, 2H, Por-β); HRMS (FAB) found *m*/*z* 1952,92(6), calcd for $C_{124}H_{140}N_8Pd_2$, *m*/*z* 1952.9270; UV/visible ($CHCl_3$) λ_{max} (ϵ) = 420 (95 500), 544 (93 000), and 748 (61 500) nm. **7e**: mp >215−217 °C; ^{1}H NMR ($CDCl_3$) δ 1.46−1.56 (br, 36H, *t*-Bu), 1.49 (s, 36H, t-Bu), 1.55 (s, 18H, *t*-Bu), 1.56 (s, 18H, *t*-Bu), 7.73 (m, *J* = 1.8 H z,

(33) (a) Wang, Q. M.; Bruce, D. W. *Synlett* **1995**, 1267. (b) Littler, B. J.; Ciringh, Y.; Lindsey, J. S. *J. Org. Chem.* **1999**, *64*, 2864.

4H, Ar-H), 7.75 (t, J = 1.8 Hz, 1H, Ar-H), 7.79 (d, J = 1.8 Hz, 2H, Ar-H), 7.85−8.12 (br; 5H, Ar-H), 7.91 (d, J = 1.8 Hz, 2H, Ar-H), 7.93 (d, J = 1.8 Hz, 2H, Ar-H), 7.99 (s, 2H, Ar-H)), 8.44 (d, J = 1.8 Hz, 1H, Por-β), 8.46 (s, 3H, Por-β), 8.47 (d, J = 4.9 Hz, 1H, Por-β), 8.49 (d, J = 4.9 Hz, 1H, Por-β), 8.52 (d, J = 4.9 Hz, 1H, Por-β), 8.55 (d, J = 4.9 Hz, 1H, Por-β), 8.56 (d, J = 4.9 Hz, 1H, Por-β), 8.75 (d, J = 4.9 Hz, 1H, Por-β), 9.13 (s, 1H, Por-β), 9.64 (d, J = 4.9 Hz, 1H, Por-β), 9.65 (d, J = 4.9 Hz, 1H, Por-β); HRMS (FAB) found m/z 1986.82(9) calcd for $C_{124}H_{139}ClN_8Pd_2$, m/z 1986.8881; UV/visible ($CHCl_3$) λ_{max} = 423, 543, and 747 nm. **7f**: mp >217−219 °C; ^{1}H NMR ($CDCl_3$) δ 1.43−1.55 (br, 72H, *t*-Bu), 1.48 (s, 36H, *t*-Bu), 7.66 (t, J = 1.8 Hz, 2H, Ar-H), 7.72−7.74 (m, 4H, Ar-H), 7.70−8.00 (br, 12H, Ar-H), 8.35 (d, J = 1.8 Hz, 2H, Ar-H), 8.40 (d, J = 4.9 Hz, 2H, Por-β), 8.47 (s, 4H, Por-β), 8.53 (d, J = 4.9 Hz, 2H, Por-β), and 9.50 (d, J = 4.9 Hz, 2H, Por-β); HRMS (FAB) found m/z 2020.92(7), calcd for $C_{124}H_{138}Cl_2N_8Pd_2$, m/z 2020.8491; UV/visible ($CHCl_3$) λ_{max} = 426, 542, and 734 nm.

Meso-β Doubly Linked Free-Base Diporphyrin 7g. The meso-β doubly linked Cu^{II}−diporphyrin **7c** (30 mg, 16 μmol) was dissolved in a mixture of $CHCl_3$, TFA, and 10% H_2SO_4. After being stirred for 30 min, the mixture was poured into water and the porphyrin products were extracted with $CHCl_3$. The combined organic extract was washed with water, aqueous $NaHCO_3$, and brine and dried over Na_2SO_4. Separation by chromatography through an alumina column gave the corresponding meso-β doubly linked free-base diporphyrin **7g** (25 mg, 90%). **7g**: mp >300 °C; ^{1}H NMR ($CDCl_3$) δ 0.62 (s, 4H, NH), 1.50 (s, 36H, *t*-Bu), 1.56 (s, 36H, *t*-Bu), 1.61 (s, 36H, *t*-Bu), 7.74 (t, J = 1.8 Hz, 2H, Ar-H), 7.79 (t, J = 1.8 Hz, 2H, Ar-H), 7.84 (t, J = 1.8 Hz, 2H, Ar-H), 7.95 (d, J = 1.8 Hz, 4H, Ar-H), 8.02 (d, J = 1.8 Hz, 4H, Ar-H), 8.15 (d, J = 1.8 Hz, 4H, Ar-H), 8.42 (d, J = 4.9 Hz, 2H, Por-β), 8.44 (d, J = 4.9 Hz, 2H, Por-β), 8.47 (d, J = 4.9 Hz, 2H, Por-β), 8.53 (d, J = 4.9 Hz, 2H, Por-β), 8.63 (d, J = 4.9 Hz, 2H, Por-β), 9.18 (s, 2H, Por-β), and 9.55 (d, J = 4.9 Hz, 2H, Por-β); HRMS (FAB) found m/z 1745.12(3), calcd for for $C_{124}H_{144}N_8$, m/z 1745.1514; UV/visible ($CHCl_3$) λ_{max} (ϵ) = 425 (144 500), 501 (75 400), 546 (61 600), 616 (49 900), and 820 (67 800) nm.

Meso-β Doubly Linked Zn^{II}−Diporphyrin 7h. The meso-β doubly linked free-base diporphyrin **7g** (42 mg, 24 μmol) was converted to Zn^{II}−diporphyrin **7h** (42 mg, 93%) by the standard method. **7h**: mp >300 °C; ^{1}H NMR ($CDCl_3$) δ 1.51 (s, 36H, *t*-Bu), 1.57 (s, 36H, *t*-Bu), 1.62 (s, 36H, *t*-Bu), 7.73 (t, J = 1.8 Hz, 2H, Ar-H), 7.79 (t, J = 1.8 Hz, 2H, Ar-H), 7.83 (t, J = 1.8 Hz, 2H, Ar-H), 7.96 (d, J = 1.8 Hz, 4H, Ar-H), 8.04 (d, J = 1.8 Hz, 4H, Ar-H), 8.19 (d, J = 1.8 Hz, 4H, Ar-H), 8.56 (d, J = 4.9 Hz, 4H, Por-β), 8.60 (d, J = 4.9 Hz, 2H, Por-β), 8.65 (d, J = 4.9 Hz, 2H, Por-β), 8.77 (d, J = 4.9 Hz, 2H, Por-β), 9.37 (s, 2H, Por-β), and 9.77 (d, J = 4.9 Hz, 2H, Por-β); HRMS (FAB) found m/z 1868.97(8), calcd for $C_{124}H_{140}N_8Zn_2$, m/z 1868.9784; UV/visible ($CHCl_3$) λ_{max} (ϵ) = 424 (157 400), 496 (74 000), 562 (88 900), and 798 (75 000) nm.

Pd^{II}−Porphyrin Tetramer 7i. Meso-monobrominated meso−meso linked diporphyrin **5d** (5 mg, 3 μmol) was oxidized with BAHA (3 mg, 3.6 μmol) in 20 mL of $CHCl_3$ for 24 h at room temperature. The products were separated into tetraporphyrin and diporphyrin fractions by SEC. The latter fraction was further separated by flash chromatography over a silica gel (Wakogel FC40) column and was identified as meso-brominated diporphyrin **5e** (3 mg, 60%) and recovered **5d** (1 mg, 20%). The former was further purified by flash chromatography to give **7i** (1 mg, 20%) over a silica gel column (Wakogel FC40). **7i**: mp >300 °C; ^{1}H NMR ($CDCl_3$) δ 1.43 (s, 36H, *t*-Bu), 1.47 (s, 72H, *t*-Bu), 1.48 (s, 36H, *t*-Bu), 7.66(d, J = 4.9 Hz, 4H, Por-β), 8.51 (d, J = 4.9 Hz, 2H, Por-β), 8.58 (d, J = 4.9 Hz, 2H, Por-β), 7.70 (t, J = 1.8 Hz, 2H, Ar-H), 7.74 (t, J = 1.8 Hz, 4H, Ar-H), 7.77 (t, J = 1.8 Hz, 2H, Ar-H), 8.00 (d, J = 1.8 Hz, 4H, Ar-H), 8.03 (d, J = 1.8 Hz, 8H, Ar-H), 8.17 (d, J = 1.8 Hz, 4H, Ar-H), 8.26 (d, J = 4.9 Hz, 2H, Por-β), 8.34 (d, J = 4.9 Hz, 2H, Por-β), 8.64 (d, J = 4.9 Hz, 4H, Por-β), 8.81 (d, J = 4.9 Hz, 2H, Por-β), 8.96 (d, J = 4.9 Hz, 4H, Por-β), 9.42 (s, 2H, Por-β), 9.74 (d, J = 4.9 Hz, 4H, Por-β),and 9.83 (d, J = 4.9 Hz, 2H, Por-β); MALDI-TOF MS m/z 3319; calcd for $C_{192}H_{198}Br_2N_{16}Pd_4$, m/z 3315; UV/visible ($CHCl_3$) λ_{max} = 419, 554, 752 and 1036 nm.

Meso−Meso β−β β−β Triply Linked Cu^{II}−Diporphyrin 8a. A 50-mL round-bottomed flask was charged with a suspension of **5c** (19 mg, 10 μmol) in C_6F_6 (20 mL). The reaction vessel was covered with foil and then BAHA (25 mg, 30 μmol) was added in one portion. After being stirred for 2 days at room temperature, the reaction mixture was diluted with a mixture of methanol and THF. The solvent was removed on a rotary evaporator, and the residue was precipitated by treatment with a mixture of benzene and methanol. The product was finally separated by flash chromatography on silica gel (Wakogel C-400). Elution with hexane/CH_2Cl_2 (95:5) gave recovered **5c** (2 mg, 10%) as the first fraction, monochlorinated **8b** (3 mg, 16%) as the second fraction, and **8a** (14 mg, 74%) as the third fraction. **8a**: mp >300 °C; HRMS (FAB) found m/z 1865.01(5), calcd for $C_{124}H_{138}N_8Cu_2$, m/z 1864.9836; UV/visible ($CHCl_3$) λ_{max} (ϵ) = 411 (150 800), 576 (131 400), and 996 (35 200) nm. **8b**: mp >300 °C; HRMS (FAB) found m/z 1898.84(9), calcd for $C_{124}H_{137}ClN_8Cu_2$, m/z 1898.9447; UV/visible ($CHCl_3$) λ_{max} = 409, 573, and 990 nm.

Meso−Meso β−β β−β Triply Linked Free-Base Diporphyrin 8c. Triply linked Cu^{II}−diporphyrin **8a** (13 mg, 7.0 μmol) was dissolved in a mixture of $CHCl_3$ and concentrated H_2SO_4. After being stirred for 30 min, the mixture was poured into water and the porphyrin products were extracted with $CHCl_3$. The combined organic extracts were washed with water, aqueous $NaHCO_3$, and brine and dried over Na_2SO_4. Separation by silica gel column chromatography gave the corresponding triply linked free-base diporphyrin **8c** (9 mg, 74%). **8c**: mp >300 °C; ^{1}H NMR ($CDCl_3$) δ 1.41 (s, 36H, *t*-Bu), 1.42 (s, 4H, NH), 1.45 (s, 72H, *t*-Bu), 7.36 (s, 4H, Por-β), 7.59 (t, J = 1.8 Hz, 2H, Ar-H), 7.60 (d, J = 4.9 Hz, 4H, Por-β), 7.62 (t, J = 1.8 Hz, 4H, Ar-H), 7.63 (d, J = 4.9 Hz, 4H, Por-β), 7.65 (d, J = 4.9 Hz, 4H, Por-β), and 7.67 (d, J = 1.8 Hz, 8H, Ar-H); HRMS (FAB) found m/z 1743.10(4), calcd for $C_{124}H_{142}N_8$, m/z 1743.1357; UV/visible ($CHCl_3$) λ_{max} (ϵ) = 410 (117 900), 567 (112 200), and 1086 (26 800) nm.

Meso−Meso β−β β−β Triply Linked Zn^{II}−Diporphyrin 8d. Triply linked free-base diporphyrin **8c** (10 mg, 5.7 μmol) was converted to Zn^{II}−diporphyrin **8d** (10 mg, 93%) by the standard method. **8d**: mp >300 °C; ^{1}H NMR ($CDCl_3$) δ 1.41 (s, 36H, *t*-Bu), 1.45 (s, 72H, *t*-Bu), 7.35 (s, 4H, Por-β), 7.59 (t, J = 1.8 Hz, 2H, Ar-H), 7.61(t, J = 1.8 Hz, 4H, Ar-H), 7.63 (d, J = 1.8 Hz, 4H, Ar-H), 7.67 (d, J = 1.8 Hz, 8H, Ar-H), 7.70 (d, J = 4.9 Hz, 4H, Por-β), and 7.75 (d, J = 4.9 Hz, 4H, Por-β); HRMS (FAB) found m/z 1866.94(4), calcd for $C_{124}H_{138}N_8Zn_2$, m/z 1866.9627; UV/visible ($CHCl_3$) λ_{max} (ϵ) = 419 (113 000), 582 (101 600), and 1068 (22 900) nm.

Meso−Meso β−β β−β Triply Linked Ni^{II}−Diporphyrin 8e and Meso−Meso β−β Doubly Linked Ni^{II}−Diporphyrin 9a. The porphyrin **5a** (10 mg, 5.4 μmol) was oxidized with BAHA (9 mg, 11 μmol) in 20 mL of C_6F_6 for 2 days at room temperature. The product was separated by flash chromatography on silica gel (Wakogel C-400). Elution with hexane/CH_2Cl_2 (95:5) gave recovered **5a** (3 mg, 30%) as the first fraction, monochlorinated **9b** (2 mg, 20%) as the second fraction, monochlorinated **8l** (2 mg, 20%) as the third fraction, **9a** (1 mg, 10%) as the fourth fraction, and **8e** (1 mg, 10%) as the fifth fraction. **8e**: mp >300 °C; ^{1}H NMR ($CDCl_3$) δ 1.40 (s, 36H, *t*-Bu), 1.43 (s, 72H, *t*-Bu), 7.54 (s, 4H, Por-β), 7.57−7.60 (m, 18H, Ar-H), 7.73 (d, J = 4.9 Hz, 4H, Por-β), and 7.77 (d, J = 4.9 Hz, 4H, Por-β); HRMS (FAB) found m/z 1854.91(3), calcd for $C_{124}H_{138}N_8Ni_2$, m/z 1854.9751; UV/visible ($CHCl_3$) λ_{max} (ϵ) = 408 (76 900), 575 (82 500), and 933 (12 000) nm. **8l**: mp >300 °C; ^{1}H NMR ($CDCl_3$) δ 1.39 (s, 18H, *t*-Bu), 1.40 (s, 18H, *t*-Bu), 1.41 (s, 18H, *t*-Bu), 1.42 (s, 18H, *t*-Bu), 1.43 (s, 36H, *t*-Bu), and complicated overlapping Por-β and Ar protons in the range of 7.40−7.85 ppm; HRMS (FAB) found m/z 1888.87(4), calcd for $C_{124}H_{137}ClN_8Ni_2$, m/z 1888.9362; UV/visible ($CHCl_3$) λ_{max} = 408, 575, and 932 nm. **9a**: mp >300 °C; ^{1}H NMR ($CDCl_3$) δ 1.33−1.43 (br, 108H, *t*-Bu), 7.43 (d, J = 4.9 Hz, 2H, Por-β), 7.56 (t, J = 1.8 Hz, 2H, Ar-H), 7.61 (t, J = 1.8 Hz, 2H, Ar-H), 7.67 (t, J = 1.8 Hz, 2H, Ar-H), 8.42−8.44 (m, 8H, Por-β), 8.47 (d, J = 4.9 Hz, 2H, Por-β), and 8.77 (s, 2H, Por-β); HRMS (FAB) found m/z 1856.90(8), calcd for $C_{124}H_{140}N_8Ni_2$, m/z 1856.9908; UV/visible ($CHCl_3$) λ_{max} (ϵ) = 410 (57 200), 490 (77 200), and 735 (40 300) nm. **9b**: mp >300 °C; ^{1}H NMR ($CDCl_3$) δ 1.40−1.50 (br, 108H, *t*-Bu), 7.02 (t, J = 1.8 Hz, 1H, Ar-H), 7.47 (d, J = 4.9 Hz, 2H, Por-β), 7.63 (m, 2H, Ar-H), 7.69 (d, J = 1.8 Hz, 2H, Ar-H), 7.70 (t, J = 1.8 Hz, 1H, Ar-H), 7.71 (t, J = 1.8 Hz, 1H, Ar-H), 8.41 (t, J = 1.8 Hz, 1H, Ar-H), 8.48−8.52 (m, 7H, Por-β), 8.54 (d, J = 4.9 Hz, 1H, Por-β), 8.56 (d, J = 4.9 Hz, 1H,

Table 3. Crystal Data and Structure Refinements of **7b**, **7c**, **8g**, **8j** and **9a**[a]

ID code	**7b**	**7c**	**8g**	**8j**	**9a**
chem formula	$C_{124}H_{140}N_8Ni_2 \cdot 2C_6H_{14}$	$C_{124}H_{140}N_8Cu_2 \cdot 4C_6H_6$	$C_{108}H_{106}Cu_2N_8 \cdot 2C_6H_6$	$C_{108}H_{106}Zn_2N_8 \cdot C_6H_6 \cdot 2C_2H_6O$	$C_{124}H_{140}N_8Ni_2$
formula wt	2029.21	2179.19	1796.83	1720.76	1856.99
temp, K	105	296	296	296	296
wavelength, Å	0.710 69	0.710 69	0.7107	0.7107	0.710 69
cryst syst	triclinic	triclinic	monoclinic	triclinic	triclinic
space group	*P*-1	*P*-1	*C*2/*c*	*P*-1	*P*-1
unit cell dimens					
a, Å	14.807(1)	16.2904(5)	44.268(2)	17.428(7)	19.9822(9)
b, Å	15.293(1)	17.5885(3)	17.791(6)	20.324(2)	29.361(1)
c, Å	16.595(1)	13.378(1)	17.326(5)	8.566(2)	12.8584(4)
α, deg	68.256(4)	95.848(5)	90	91.696(2)	99.425(1)
β, deg	77.287(5)	101.181(6)	98.365(2)	96.988(4)	102.2310(4)
γ, deg	75.368(5)	94.798(5)	90	99.278(4)	105.9260(6)
volume, Å^3	3344	3719	13500	2968	6889.3
Z	1	1	6	1	2
density (calcd), g/cm^3	1.09	0.97	1.21	1.02	0.90
abs coeff, cm^{-1}	3.33	3.31	5.26	4.51	3.14
F(000)	1196	1166	5964	964	1992
cryst size, mm^3	0.20 × 0.30 × 0.25	0.50 × 0.30 × 0.1	0.30 × 0.30 × 0.05	0.30 × 0.20 × 0.1	0.40 × 0.20 × 0.10
$2\theta_{max}$, deg	52.7	55.0	55.0	55.0	55.0
obsd reflctns	8446	7564	3555	4134	10877
total reflctns	11968	16058	15223	11695	28184
completeness to $\theta = 55.0°$, %	100.0	100.0	100.0	100.0	100.0
absorpn corrn	empirical	empirical	empirical	empirical	empirical
refinement method	full-matrix least-squares on F^2	full-matrix least-squares on F^2	full-matrix least-squares on F^2	Full-matrix least-squares on F^2	Full-matrix least-squares on F^2
Data/restraints/params	8446/0/616	7564/0/604	3555/0/557	4134/0/568	10877/0/883
goodness of fit on F^2	5.17	0.86	2.42	3.19	0.97
final *R* indices [I>3σ(*I*)]	$R_1 = 0.093$, $wR_2 = 0.114$	$R_1 = 0.098$, $wR_2 = 0.136$	$R_1 = 0.096$, $wR_2 = 0.137$	$R_1 = 0.098$, $wR_2 = 0.119$	$R_1 = 0.123$, $wR_2 = 0.212$
largest diff peak and hole, e/Å^3	2.50 and −0.63	0.70 and −0.63	0.68 and −0.40	1.21 and −0.55	1.50 and −1.91

[a] Hydrogen atom treatment: Hydrogen atoms were generated by their idealized geometry and refined with a riding model with the exception of the following:

Por-*β*), 8.61 (d, *J* = 4.9 Hz, 1H, Por-*β*), and 9.35 (s, 1H, Por-*β*); HRMS (FAB) found *m*/*z* 1890.95(9), calcd for $C_{124}H_{139}ClN_8Ni_2$, *m*/*z* 1890.9518; UV/visible ($CHCl_3$) $\lambda_{max}(\epsilon)$ = 407 (60 800), 492 (74 000), and 728 (32 000) nm.

Meso−Meso *β*−*β* *β*−*β* Triply Linked Pd^{II}−Porphyrin 8f. The triply linked free-base diporphyrin **8c** (10 mg, 5.7 *μ*mol) was converted to **8f** (9 mg, 80%) by the standard method. **8f**: mp >300 °C; ^{1}H NMR ($CDCl_3$) *δ* 1.43 (s, 36H, t-Bu), 1.47 (s, 72H, t-Bu), 7.36 (s, 4H, Por-*β*), 7.59−7.67 (m, 10H, Ar-H), 7.69 (s, 4H, Por-*β*), 7.74 (d, *J* = 1.8 Hz, 8H, Ar-H), and 7.83 (s, 4H, Por-*β*); HRMS (FAB) found *m*/*z* 1950.91(7), calcd for $C_{124}H_{138}N_8Pd_2$, *m*/*z* 1950.9114; UV/visible ($CHCl_3$) $\lambda_{max}(\epsilon)$ = 408 (147 400), 569 (205 500), and 935 (31 900) nm.

Meso−Meso *β*−*β* *β*−*β* Triply Linked Cu^{II}−Diporphyrin 8g. The porphyrin **5f** (16 mg, 10 *μ*mol) was oxidized with BAHA (18 mg, 22 *μ*mol) in 20 mL of C_6F_6 for 2 days at room temperature. The product was finally separated by flash chromatography on silica gel (Wakogel C-400). Elution with hexane/CH_2Cl_2 (95:5) gave recovered **5f** (2 mg, 13%) as the first fraction, monochlorinated **8h** (1.0 mg, 6%) as the second fraction, and **8g** (12.2 mg, 76%) as the third fraction. **8g**: mp >300 °C; HRMS (FAB) found *m*/*z* 1640.71(5), calcd for $C_{108}H_{106}N_8Cu_2$, *m*/*z* 1640.7332; UV/visible ($CHCl_3$) λ_{max} (ϵ) = 411 (161 800), 575 (136 100), and 994 (38 700) nm. The diporphyrin **8g** was demetalated to free-base diporphyrin **8i**. **8i**: mp >300 °C; ^{1}H NMR ($CDCl_3$) *δ* 1.45 (s, 72H, t-Bu), 1.51(s, 4H, NH), 7.55 (d, *J* = 4.9 Hz, 4H, Por-*β*), 7.56 (s, 4H, Por-*β*), 7.58 (s, 10H, Ar-H), 7.62 (t, *J* = 1.8 Hz, 4H, Ar-H), 7.64 (d, *J* = 1.8 Hz, 8H, Ar-H), and 7.79 (d, *J* = 4.9 Hz, 4H, Por-*β*). HRMS (FAB) found *m*/*z* 1518.91(7), calcd for $C_{108}H_{110}N_8$, *m*/*z* 1518.8853; UV/visible ($CHCl_3$) $\lambda_{max}(\epsilon)$ = 410 (119 300), 567 (114 400), and 1086 (26 100) nm. **8h**: mp >300 °C; HRMS (FAB) found *m*/*z* 1674.68(2), calcd for $C_{108}H_{105}ClN_8Cu_2$, *m*/*z* 1674.6943; UV/visible ($CHCl_3$) $\lambda_{max}(\epsilon)$ = 409, 573, and 993 nm.

Monochlorinated Meso−Meso *β*−*β* *β*−*β* Triply Linked Diporphyrin 8k. Triply linked Cu^{II}−diporphyrin **8b** (10 mg, 5.3 *μ*mol) was dissolved in a mixture of $CHCl_3$ and concentrated H_2SO_4. After being stirred for 30 min, the mixture was poured into water and the porphyrin products were extracted with $CHCl_3$. The combined organic extracts were washed with water, aqueous $NaHCO_3$, and brine and dried over Na_2SO_4. Separation by silica gel column chromatography gave the corresponding triply linked free-base diporphyrin **8k** (8 mg, 85%). The structure of **8k** was determined in X-ray crystallography (Supporting Information 3). **8k**: mp >300 °C; ^{1}H NMR ($CDCl_3$) *δ* 1.41 (s, 18H, *t*-Bu), 1.42 (s, 18H, *t*-Bu), 1.43 (s, 18H, *t*-Bu), 1.44 (s, 18H, *t*-Bu), 1.45 (s, 36H, *t*-Bu), and complicated overlapping Por-*β* and Ar protons in the range of 7.45−7.75 ppm; HRMS (FAB) found *m*/*z* 1777.08(3), calcd for $C_{124}H_{141}ClN_8$, *m*/*z* 1777.0968; UV/visible ($CHCl_3$) $\lambda_{max}(\epsilon)$ = 408 (121 000), 567 (116 000), and 1081 (27 500) nm.

Meso−Meso *β*−*β* *β*−*β* Triply Linked Zn^{II}−Diporphyrin 8j. The triply linked Cu^{II}−diporphyrin **8g** (5 mg, 3.1 *μ*mol) was demetalated by stirring in a mixture of $CHCl_3$, concentrated H_2SO_4 for 30 min to provide the corresponding free-base diporphyrin, from which Zn^{II}−diporphyrin **8j** was prepared by the standard method (4 mg, 80%). **8j**: mp >300 °C; ^{1}H NMR ($CDCl_3$) *δ* 1.45 (s, 72H, *t*-Bu), 7.35 (s, 4H, Por-*β*), 7.56 (d, *J* = 4.9 Hz, 4H, Por-*β*), 7.62 (t, *J* = 1.8 Hz, 4H, Ar-H), 7.66 (d, *J* = 1.8 Hz, 8H, Ar-H), 7.69 (s, 10H, Ar-H), and 7.80 (d, *J* = 4.9 Hz, 4H, Por-*β*); HRMS (FAB) found *m*/*z* 1642.67(3), calcd for $C_{108}H_{106}N_8Zn_2$, *m*/*z* 1642.7123; UV/visible ($CHCl_3$) $\lambda_{max}(\epsilon)$ = 418 (10 800), 581 (91 000), and 1068 (19 700) nm.

Crystal Structure Data for 7b, 7c, 8 g, 8j, and 9a. Data of the crystal structure of **7b**·$2C_6H_{14}$: $C_{136}H_{168}Ni_2N_8$, M_W = 2029, crystal from $CHCl_3/C_6H_{14}$, crystal dimensions 0.2 × 0.3 × 0.25 mm, space group *P*-1, *a* = 14.807 (1) Å, *b* = 15.293 (1) Å, *c* = 16.595 (1) Å, α = 68.256 (4)°, *β* = 77.287 (5)°, *γ* = 75.368 (5)°, *V* = 3344 Å^3. *Z* = 1, ρ_{calc} = 1.09 g cm^{-3}; μ_{Mo} = 3.23 cm^{-1}; θ_{max} = 27.5°. For 11 968

reflections measured; $R_1 = 0.093$ for 8446 data [$I > 3\sigma(I)$], $wR_2 = 0.114$ for all measured data. (See Table 3.)

Data of the crystal structure of **7c**·$4C_6H_6$: $C_{148}H_{164}Ni_2N_8Cu_2$, $M_W = 2182$, crystal from C_2H_5OH/C_6H_6, crystal dimensions $0.5 \times 0.3 \times 0.1$ mm, space group *P*-1, $a = 16.2904$ (5) Å, $b = 17.5885(3)$ Å, $c = 13.378(1)$ Å, $\alpha = 95.848(5)°$, $\beta = 101.181(6)°$, $\gamma = 94.798(2)°$, $V = 3719.7(3)$ Å^3. $Z = 1$, $\rho_{calc} = 0.974$ g cm^{-3}; $\mu_{Mo} = 3.31$ cm^{-1}; $\theta_{max} = 27.5°$. For 16 058 reflections measured; $R_1 = 0.098$ for 7564 data [$I > 3\sigma(I)$], $wR_2 = 0.136$ for all measured data.

Data of the crystal structure of **8g**·$2C_6H_6$: $C_{120}H_{118}Cu_2N_8$, $M_W = 1796$, crystal from C_6H_6/C_2H_5OH, crystal dimensions $0.3 \times 0.3 \times 0.1$ mm, space group *C*2/*c*, $a = 44.268$ (2) Å, $b = 17.791$ (6) Å, $c = 17.326$ (5) Å, $\alpha = 90°$, $\beta = 98.365$ (2)°, $\gamma = 90°$, $V = 13500$ Å^3. $Z = 6$, $\rho_{calc} = 1.21$ g cm^{-3}; $\mu_{Mo} = 5.26$ cm^{-1}; $\theta_{max} = 27.5°$. For 15 223 reflections measured; $R_1 = 0.096$ for 3555 data [$I > 3\sigma(I)$], $wR_2 = 0.137$ for all measured data.

Data of the crystal structure of **8j**·C_6H_6·$2C_2H_6O$: $C_{118}H_{124}N_8O_2Zn_2$, $M_W = 1817$, crystal from C_6H_6/C_2H_5OH, crystal dimensions $0.3 \times 0.3 \times 0.1$ mm, space group *P*-1, $a = 17.428$ (7) Å, $b = 20.324$ (2) Å, $c = 8.566$ (2) Å, $\alpha = 91.696$ (2)°, $\beta = 96.988$ (4)°, $\gamma = 99.278$ (4)°, $V = 2968$ Å^3. $Z = 1$, $\rho_{calc} = 1.02$ gcm^{-3}; $\mu_{Mo} = 4.51$ cm^{-1}; $\theta_{max} = 27.5°$. For 11 695 reflections measured; $R_1 = 0.098$ for 4134 data [$I > 3\sigma(I)$], $wR_2 = 0.119$ for all measured data.

Data of the crystal structure of **9a**: $C_{124}H_{140}Ni_2N_8$, $M_W = 1857$, crystal from C_7H_8/C_2H_6O, crystal dimensions $0.4 \times 0.2 \times 0.1$ mm, space group *P*-1, $a = 19.9822$ (9) Å, $b = 29.361$ (1) Å, $c = 12.8584$ (4) Å, $\alpha = 99.425$ (1)°, $\beta = 102.2310$ (4)°, $\gamma = 105.9260$ (6)°, $V = 6889.3$ Å^3. $Z = 2$, $\rho_{calc} = 0.940$ g cm^{-3}; $\mu_{Mo} = 3.16$ cm^{-1}; $\theta_{max} = 27.5°$. For 28 184 reflections measured; $R_1 = 0.123$ for 10877 data [$I > 3\sigma(I)$], $wR_2 = 0.212$ for all measured data.

Diffraction data of **7b** were collected on a Mac Science DIP-2020K imaging plate system diffractometer (105 K, Mo Kα radiation $\lambda = 0.7107$ Å). Whereas, diffraction data for **7c**, **8g**, **8j**, and **9a** were collected on a Rigaku−Raxis imaging plate system diffractometer (296 K, Mo Kα radiation $\lambda = 0.7107$ Å).

The structures of all the compounds were solved by direct methods and refined by F^2 with all observed reflections. All non-hydrogen atoms were refined anisotropically, and hydrogen atoms were added to calculated positions. The programs used were structure determination by SIR92 and refined by teXane for Windows.

Acknowledgment. This work was supported by Grant-in-Aids for Scientific Research from the Ministry of Education, Science, Sports and Culture of Japan (11223205, 12440196, and 12874076) and by CREST (Core Research for Evolutional Science and Technology) of Japan Science and Technology Corporation (JST). A.T. thanks JSPS for a Research Fellowship for Young Scientists. We thank Prof. M. Inouye (Toyama Medical and Pharmaceutical University) for his help in measurements of the CD spectra.

Supporting Information Available: Preliminary X-ray structures of **7f** and **8k**, absorption spectrum of **7i**, racemization experimental data on **9a**, and X-ray structural details on **7b**, **7c**, **8g**, **8j**, and **9a**. This material is available free of charge via the Internet at http://pubs.acs.org. See any current masthead page for ordering information and Web access instructions.

JA0110933